Article

Cell Reports

The Splicing Factor hnRNP M Is a Critical Regulator of Innate Immune Gene Expression in Macrophages

Graphical Abstract

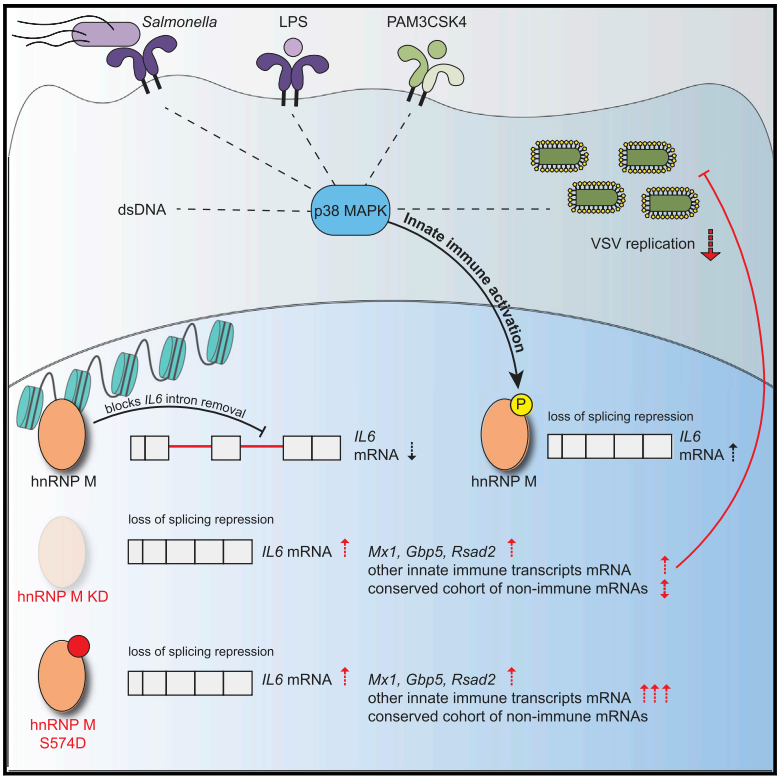

Highlights

- hnRNP M represses a cohort of innate immune transcripts in macrophages
- hnRNP M associates with the *IL6* genomic locus to co-transcriptionally repress splicing
- Following infection, phosphorylation of hnRNP M at S574 can relieve this repression
- Loss of hnRNP M enhances macrophages' ability to control viral infection

Authors

Kelsi O. West, Haley M. Scott, Sylvia Torres-Odio, A. Phillip West, Kristin L. Patrick, Robert O. Watson

Correspondence

kpatrick03@tamu.edu (K.L.P.), robert.watson@tamu.edu (R.O.W.)

In Brief

West et al. report that hnRNP M represses expression of a cohort of innate immune transcripts in infected macrophages. *IL6* splicing repression is relieved when hnRNP M is phosphorylated at specific residues, demonstrating that post-translational modification of splicing factors downstream of pathogen sensing can control maturation of innate immune mRNAs.

West et al., 2019, Cell Reports *29*, 1594–1609
November 5, 2019
https://doi.org/10.1016/j.celrep.2019.09.078

CellPress

OPEN ACCESS
CellPress

Cell Reports
Article

The Splicing Factor hnRNP M Is a Critical Regulator of Innate Immune Gene Expression in Macrophages

Kelsi O. West,[1] Haley M. Scott,[1] Sylvia Torres-Odio,[1] A. Phillip West,[1] Kristin L. Patrick,[1,*] and Robert O. Watson[1,2,*]
[1]Department of Microbial Pathogenesis and Immunology, Texas A&M Health Science Center, Bryan, TX 77807, USA
[2]Lead Contact
*Correspondence: kpatrick03@tamu.edu (K.L.P.), robert.watson@tamu.edu (R.O.W.)
https://doi.org/10.1016/j.celrep.2019.09.078

SUMMARY

While transcriptional control of innate immune gene expression is well characterized, almost nothing is known about how pre-mRNA splicing decisions influence, or are influenced by, macrophage activation. Here, we demonstrate that the splicing factor hnRNP M is a critical repressor of innate immune gene expression and that its function is regulated by pathogen sensing cascades. Loss of hnRNP M led to hyperinduction of a unique regulon of inflammatory and antimicrobial genes following diverse innate immune stimuli. While mutating specific serines on hnRNP M had little effect on its ability to control pre-mRNA splicing or transcript levels of housekeeping genes in resting macrophages, it greatly impacted the protein's ability to dampen induction of specific innate immune transcripts following pathogen sensing. These data reveal a previously unappreciated role for pattern recognition receptor signaling in controlling splicing factor phosphorylation and establish pre-mRNA splicing as a critical regulatory node in defining innate immune outcomes.

INTRODUCTION

When innate immune cells like macrophages sense pathogens, they undergo a massive reprogramming of gene expression. Although innate immune gene expression is mostly studied in the context of transcriptional activation, multiple lines of evidence support a crucial role for pre-mRNA splicing regulation in shaping the macrophage transcriptome. For example, when primary mouse macrophages are treated with a Toll-like receptor 4 (TLR4) agonist, individual transcripts show significant variation in the time it takes for them to be fully spliced, with some pre-mRNAs remaining unprocessed for hours after transcriptional activation (Bhatt et al., 2012; Pandya-Jones et al., 2013). Likewise, computational analyses of human primary macrophages reveal a robust increase in mRNA isoform diversity and a global preference for exon inclusion following lipopolysaccharide (LPS) treatment or *Salmonella enterica* serovar Typhimurium infection (Pai et al., 2016). The production of functionally diverse protein isoforms via alternative splicing is also known to influence innate immune responses. Several important innate immune molecules that function downstream of pattern recognition receptors, such as the TLR adaptor protein MyD88 (Janssens et al., 2003), the interleukin-1 receptor associated kinase 1, IRAK1 (Rao et al., 2005), and even some of the TLRs themselves (TLR3, TLR4 co-receptor MD2) (Gray et al., 2010; Seo et al., 2015), are regulated through expression of truncated isoforms that auto-inhibit full-length protein function and dampen inflammatory responses. In the case of MyD88, splicing factors like SF3a1 have been directly implicated in generating the MyD88 short isoform (MyD88-S), which inhibits expression of pro-inflammatory cytokines like interleukin-6 (IL-6) following LPS treatment (De Arras and Alper, 2013; De Arras et al., 2013).

To date, only a handful of RNA-binding proteins (RBPs) have been studied in the context of the innate immune response. For example, TLR4 signaling via LPS treatment promotes the shuttling of hnRNP U (heterogeneous nuclear ribonucleoprotein particle U) from the nucleus to the cytosol, resulting in differential expression of several innate immune cytokines (TNF-α, IL-6, IL-1β) via hnRNP U-dependent stabilization of cytosolic mRNAs (Zhao et al., 2012). Tristetraprolin (TTP), human antigen R (HuR), T cell intracellular antigen 1-related protein (TIAR), and hnRNP K have also been implicated in controlling gene expression in LPS-activated macrophages, with TTP and HuR regulating mRNA decay and TIAR and hnRNP K causing translational repression (Chen et al., 2013; Liepelt et al., 2014; Ostareck and Ostareck-Lederer, 2019). Phosphorylation is generally thought to control subcellular localization and protein-protein interactions between these RBPs (Allemand et al., 2005; Cobianchi et al., 1993; Huang et al., 2004; Ostareck-Lederer et al., 2002; Shin et al., 2004; Stamm, 2008), but the kinases/phosphatases responsible for modifying them and the conditions under which these modifications are controlled remain poorly understood.

Two recent publications measured macrophage protein phosphorylation following infection with the intracellular pathogens *Mycobacterium tuberculosis* (Penn et al., 2018) and *Cryptococcus neoformans* (Pandey et al., 2017). Intriguingly, a substantial number of these differentially phosphorylated peptides were derived from splicing factors. In fact, "spliceosome" was the top over-represented phosphorylated pathway in *C. neoformans*-infected cells, suggesting that post-translational modification (PTM) of splicing factors is critical for controlling

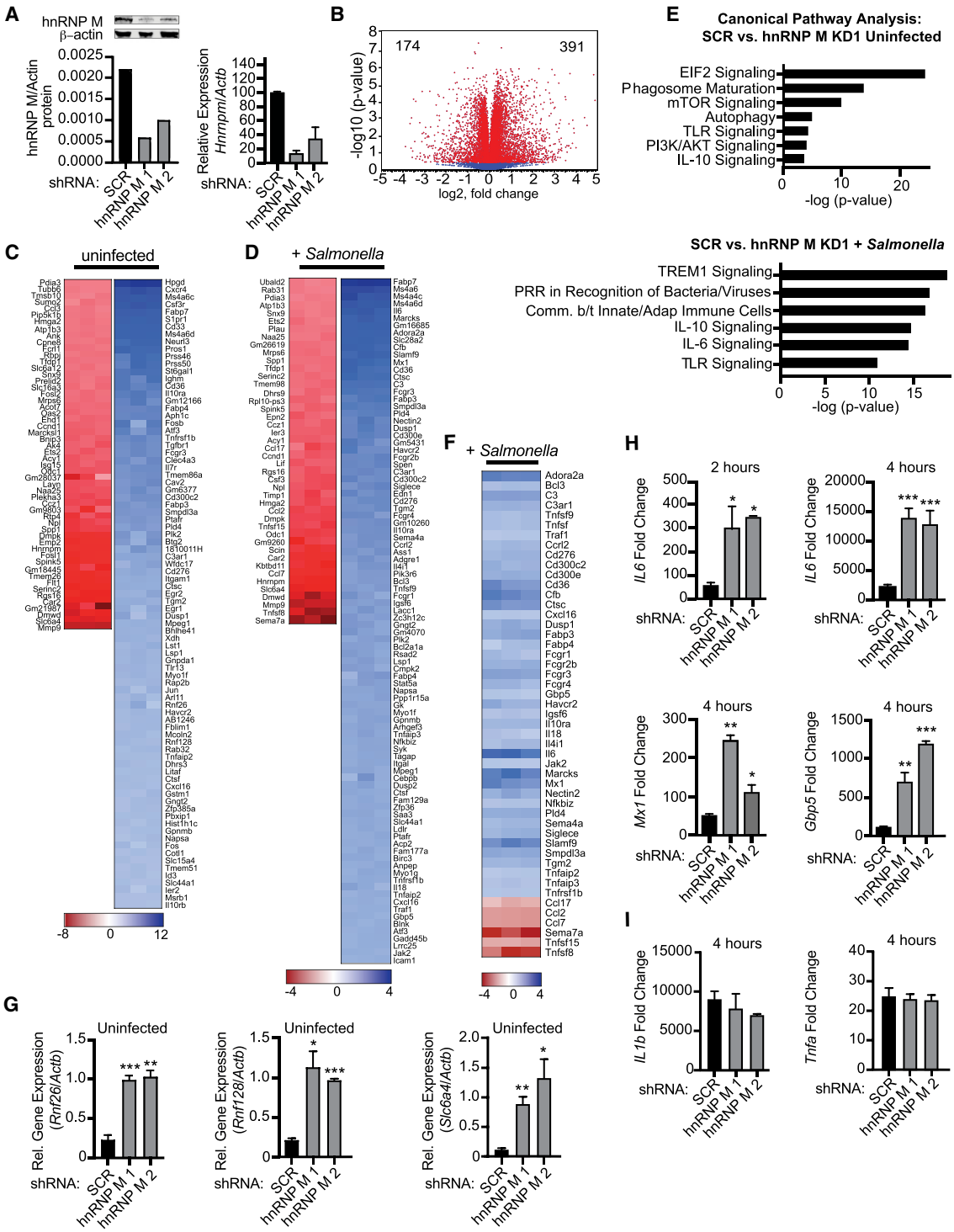

Figure 1. hnRNP M Regulates Expression of Innate Immune Genes during *Salmonella* Typhimurium Infection

(A) Western blot analysis and qRT-PCR of hnRNP M in RAW 264.7 macrophages with β-actin as a loading control. Values are mean (SD) representative of 3 biological replicates.

(B) Volcano plot (t test) showing gene expression analysis of hnRNP M KD RNA-seq data from uninfected cells. x axis shows fold change of gene expression, and y axis shows statistical significance. Downregulated genes are plotted on the left, and upregulated genes are on the right.

(C) Gene expression analysis of hnRNP M KD cells compared to SCR control for uninfected cells. Each column represents a biological replicate. Red, genes downregulated in hnRNP M KD; blue, genes upregulated in hnRNP M KD.

(legend continued on next page)

innate immune responses to pathogens. One of the proteins that was significantly differentially phosphorylated in each of these datasets was hnRNP M. hnRNP M is a splicing factor and RBP that has been repeatedly implicated in cancer metastasis (Chen et al., 2014; Passacantilli et al., 2017; Thomas et al., 2011; Xu et al., 2014) and muscle differentiation (Chen et al., 2017). Its role in regulating innate immune gene expression in macrophages is unknown, although interestingly, it has also been found to influence dengue virus replication (Viktorovskaya et al., 2016), suggesting a role in antiviral responses.

Here, we demonstrate that abrogating hnRNP M expression in a macrophage cell line leads to hyperinduction of over 100 transcripts following distinct innate immune stimuli, including infection with the gram-negative bacteria *Salmonella enterica* serovar Typhimurium, treatment with TLR2 and TLR4 agonists, and transfection of cytosolic dsDNA. While our data reveal that hnRNP M co-transcriptionally represses gene expression by influencing both constitutive and alternative splicing decisions, regulation of hnRNP M's function via phosphorylation at S574 specifically controls the protein's ability to inhibit intron removal of innate immune-activated transcripts. Consistent with its role in downregulating macrophage activation, macrophages lacking hnRNP M are better able to control viral replication, emphasizing the importance of pre-mRNA splicing regulation in modulating the innate immune response to infection.

RESULTS

RNA Sequencing (RNA-Seq) Analysis Reveals Immune Response Genes Are Regulated by hnRNP M during *Salmonella* Infection

To investigate a role for hnRNP M in regulating the innate immune response, we first tested how loss of hnRNP M globally influenced macrophage gene expression. Stably selected, constitutive hnRNP M knockdown (hnRNP M KD) cell lines were generated by transducing RAW 264.7 mouse macrophages with lentiviral short hairpin RNA (shRNA) constructs designed to target hnRNP M or a control scramble (SCR) shRNA. Western blot and qRT-PCR analysis confirmed ~80% and 60% knockdown of hnRNP M using two different shRNA constructs (KD1 and KD2, respectively) (Figure 1A). Because several attempts to knock out hnRNP M in RAW 264.7 macrophages by CRISPR/Cas9 guide RNAs (gRNAs) resulted exclusively in clones with in-frame insertions or deletions (data not shown), we concluded that hnRNP M is essential in macrophages and continued our experiments using the viable knockdown cell lines.

We next performed RNA-seq analysis on total poly(A)+ selected RNA collected from uninfected and *Salmonella* Typhimurium infected cells (MOI = 10) at the key innate immune time point of 4 h post-infection, at which time transcriptional activation downstream of both MyD88 and TRIF adapters would be expected (Yamamoto et al., 2003). Using CLC Genomics Workbench, we identified a number of genes that were differentially expressed in uninfected hnRNP M KD cells compared to SCR control cells, with 391 genes upregulated and 174 downregulated (Figure 1B). Looking specifically at transcripts with a fold change of > ±1.5 ($p < 0.05$), we observed similar numbers of impacted genes in uninfected hnRNP M KD and SCR macrophages (Figure 1C) and those infected with *Salmonella* (Figure 1D). The ratio of upregulated (blue) and downregulated (red) transcripts was also quite similar between the two conditions and consistent with previous reports of hnRNP M repressing pre-mRNA splicing (Hovhannisyan and Carstens, 2007; Marko et al., 2010). Interestingly, we observed only 25% overlap between genes that were differentially expressed in uninfected and *Salmonella*-infected macrophages, suggesting that hnRNP M has distinct modes of operation depending on the activation state of a macrophage (Figure S1A). Unbiased canonical pathways analysis revealed strong enrichment for differentially expressed genes in innate immune signaling pathways in *Salmonella*-infected hnRNP M KD cells (Figure 1E), and manual analysis of these lists revealed a number of important chemokines (e.g., *Cxcl16*, *Ccl17*, *Ccl2*, *Ccl7*), antiviral molecules (e.g., *Isg15*, *Mx1*, *Rsad2*), and pro-inflammatory cytokines (e.g., *IL6*, *Mip1a* [*Ccl3*], *IL18*) whose expression were dramatically affected by loss of hnRNP M (Figure 1F). Additional pathways enriched for hnRNP M-dependent genes can be found in Figures S1B and S1C, and a list of all impacted genes (±1.5-fold change) can be found in Table S1.

To validate the RNA-seq gene expression changes, we used qRT-PCR to measure transcript levels of genes from both lists (uninfected SCR versus hnRNP M KD and *Salmonella*-infected SCR versus hnRNP M KD). We confirmed overexpression of several genes in uninfected hnRNP M KD cells (*Rnf26*, *Rnf128*, *Slc6a4*; Figure 1G), as well as hyperinduction of transcripts in hnRNP M KD cells at 2 and 4 h post-*Salmonella* infection (*IL6*, *Mx1*, *Gbp5*, *Adora2a*, and *Marcks*) (Figures 1H and S1D). Importantly, induction of other pro-inflammatory mediators such as *IL1b* and *Tnfa* did not rely on hnRNP M (Figure 1I), suggesting that hnRNP M's ability to regulate gene expression is conferred by specificity at the transcript level, rather than being common to a transcriptional regulon (e.g., nuclear factor κB [NF-κB], IRF3, STAT1). Together, these results reveal a previously unappreciated role for hnRNP

(D) Gene expression analysis of hnRNP M KD cells compared to SCR control for *Salmonella*-infected cells. Each column represents a biological replicate.
(E) Ingenuity pathway analysis of gene expression changes in uninfected and *Salmonella*-infected cells.
(F) Manually annotated hnRNP M-dependent innate immune genes. Each column represents a biological replicate.
(G) qRT-PCR of *Rnf26*, *Rnf128*, and *Slc6a4* in uninfected hnRNP M KD cells.
(H) qRT-PCR of mature *IL6*, *Mx1*, and *Gbp5* transcripts in *Salmonella*-infected hnRNP M KD cells at 2 and 4 h post-infection.
(I) qRT-PCR of *IL1b* and *Tnfa* transcripts in *Salmonella*-infected hnRNP M KD cells at 4 h post-infection.
(G)–(I) represent 3 biological replicates ± SEM, n = 3. For all experiments in this study, statistical significance was determined using two-tailed Students' t test. *$p < 0.05$, **$p < 0.01$, ***$p < 0.001$, n.s., not significant.

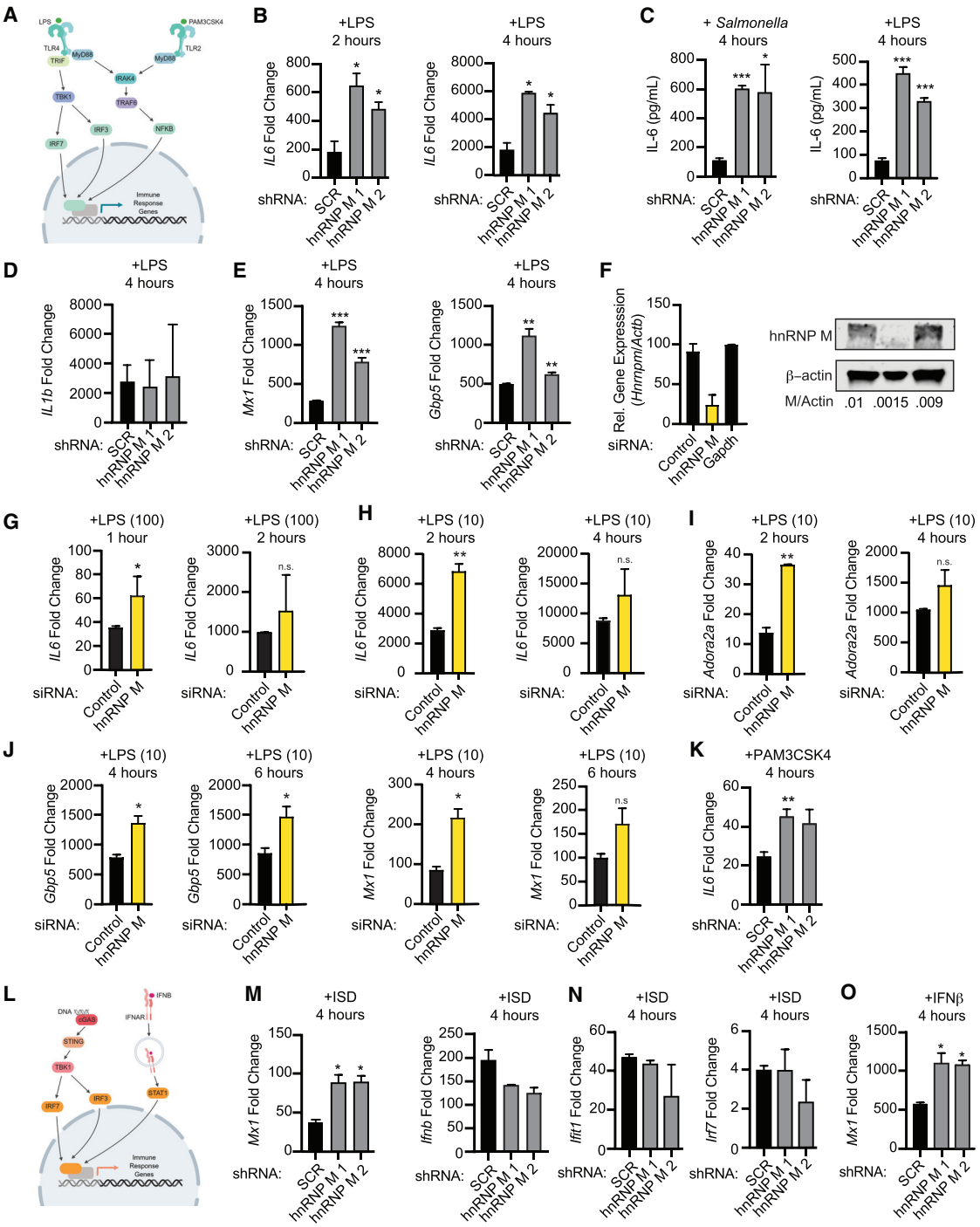

Figure 2. hnRNP M-Dependent Regulation of Innate Immune Gene Expression Occurs Downstream of Sensing Multiple Innate Immune Stimuli

(A) Model of TLR4 and TLR2 signaling.

(B) qRT-PCR of *IL6* mRNA levels in SCR control and hnRNP M KD cells treated with LPS for 2 and 4 h.

(C) IL6 ELISA with supernatants collected 4 h post-*Salmonella* infection or LPS treatment.

(D) qRT-PCR of *IL1b* transcripts in LPS-treated hnRNP M KD cells (4 h).

(E) qRT-PCR of *Mx1* and *Gbp5* mRNA levels in SCR control and hnRNP M KD cells treated with LPS (4 h).

(F) qRT-PCR and western analysis demonstrating effective depletion of hnRNP M in siRNA-transfected BMDMs. β-actin was used as a loading control.

(G) qRT-PCR of mature *IL6* in negative control and hnRNP M siRNA BMDMs treated with 100 ng/mL of LPS for 1 and 2 h.

(H) qRT-PCR of mature *IL6* in negative control and hnRNP M siRNA BMDMs treated with 10 ng/mL of LPS for 2 and 4 h.

(legend continued on next page)

M in repressing specific innate immune transcripts in macrophages.

hnRNP M Regulates a Specific Subset of Innate Immune Genes upon Treatment with Diverse Innate Immune Stimuli

Salmonella encodes several pathogen-associated molecular patterns (PAMPs) that serve as potent activators of pattern recognition receptors. *Salmonella* can also activate pro-inflammatory gene expression via its virulence-associated type III secretion system (Sun et al., 2018). To begin to determine the nature of the signal through which hnRNP M-dependent gene expression changes occur, we first tested whether LPS, a potent agonist of TLR4 (Poltorak et al., 1998) and component of the *Salmonella* outer membrane, was sufficient to hyperinduce *IL6* expression in hnRNP M KD macrophages (Figure 2A). Similar to *Salmonella* infection, we observed a 3- to 4-fold hyperinduction of *IL6* in hnRNP M KD cells treated with 100 ng/mL LPS (from *E. coli*) for 2 and 4 h, confirming that hnRNP M acts downstream of TLR4 activation (Figure 2B). Importantly, hyperinduction of *IL6* mRNA in both LPS-treated and *Salmonella*-infected hnRNP M KD macrophages increased IL-6 protein levels 3- to 6-fold (Figure 2C), indicating that hnRNP M repression of *IL6* mRNA processing impacts protein outputs in a biologically meaningful way. We believe hnRNP M mainly functions to repress *IL6* expression early in macrophage activation, as we did not observe statistically significant differences in *IL6* mRNA levels between SCR and hnRNP M KD at later time points (6 h) post-LPS treatment (Figure S2B), and this trend generally held for several other hnRNP M-dependent transcripts (Figure S2B). We did not observe any significant changes in hnRNP M protein expression over the same time course of LPS treatment (Figure S2C) nor did we observe significant differences in IκBα degradation over a course of LPS treatment in hnRNP M KD versus SCR control cells (Figure S2D), demonstrating that signaling downstream of TLR4 activation is intact in the absence of hnRNP M.

Consistent with our RNA-seq and qRT-PCR data from *Salmonella*-infected cells, *Mx1*, *Gbp5*, and *Marcks* were hyperinduced in hnRNP M KD cells after LPS treatment at 2 and 4 h (Figure 2E; Figure S2A), while *IL1b* (Figure 2D) and *Tnfa* (Figure S2A) showed no changes in expression after LPS treatment in hnRNP M KD versus SCR control cells, despite both transcripts being tremendously upregulated. Rather than being activated by NF-κB, transcription of *Mx1* and *Gbp5* occurs via STAT1 downstream of interferon (IFN)-β signaling, following IFN-β expression via the TRIF/IRF3 axis (Figure 2L). These results hinted at a mechanism for hnRNP M-dependent repression that is independent of transcription factor specificity and is instead dependent on individual transcripts.

In order to confirm that hnRNP M's ability to regulate innate immune gene expression was not unique to RAW 264.7 macrophages, we used siRNAs to knockdown hnRNP M in primary mouse bone marrow-derived macrophages (BMDMs) for 72 h, alongside negative control (designed to not target anything) and positive control (designed to target GAPDH) siRNAs (Figure 2F; Figure S2E) and treated these macrophages with LPS. Because BMDMs are incredibly responsive to innate immune agonists, we used two different concentrations of LPS, 100 ng/mL (same as in the RAW 264.7 experiments) and 10 ng/mL. In both cases, hnRNP M siRNA KD in BMDMs recapitulated the phenotype that we observed in the RAW 264.7 KD macrophages, i.e., hyperinduction of *IL6* (Figures 2G, 100 ng/mL, and 2H, 10 ng/mL), albeit with slightly different kinetics and dose responses than we observed in the RAW 264.7 cell line. Importantly, we also measured hyperinduction of *Gpb5*, *Mx1*, and *Adora2a* and no change in *Tnfa* or *IL1b* (Figures 2I, 2J, and S2F) in hnRNP M siRNA KD cells, consistent with our results in the macrophage cell line. Together, these results argue for hnRNP M playing a crucial, conserved role in innate immune gene expression in both primary murine macrophages and murine macrophage cell lines.

To more directly test the idea that hnRNP M's target specificity is at the level of the transcript itself, we tested whether genes like *Mx1* and *IL6* were hyperinduced in hnRNP M KD RAW 264.7 macrophages treated with a panel of innate immune agonists. Treatment with 100 ng/mL of the TLR2/1 agonist Pam3CSK4 hyperinduced *IL6* expression in hnRNP M KD cells compared to SCR controls (Figure 2K; Figure S2G), while *Tnfa* and *IL1b* mRNA levels remained similar (Figure S2G). Likewise, transfection of hnRNP M KD cells with 1 μg/mL IFN stimulatory DNA (ISD), a potent agonist of cytosolic DNA sensing and IRF3-mediated transcription downstream of the cGAS/STING/TBK1 axis (Stetson and Medzhitov, 2006) (Figure 2L), led to hyperinduction of *Mx1* in hnRNP M KD cells (Figure 2M). *Ifnb* and other IFN-stimulated genes (ISGs) regulated by IRF3 (*Ifit1* and *Irf7*) were expressed at similar levels (Figures 2M and 2N). Direct engagement of the IFN receptor (IFNAR) with recombinant IFN-β also resulted in *Mx1* hyperinduction in hnRNP M KD cells (Figure 2O). Collectively, these results bolster a model whereby hnRNP M represses mRNA expression of a specific subset of innate immune genes, regardless of how those genes are induced.

hnRNP M Influences Gene Expression Outcomes at the Level of Pre-mRNA Splicing

Because previous studies of hnRNP M have shown that it can enhance or silence splicing of alternatively spliced exons (Cho et al., 2014; Hovhannisyan and Carstens, 2007; Llères et al., 2010; Park et al., 2011), we first asked whether loss of hnRNP

(I) As in (H) but *Adora2a*.
(J) qRT-PCR of *Gbp5* and *Mx1* in negative control and hnRNP M siRNA BMDMs treated with 10 ng/mL of LPS for 4 and 6 h.
(K) qRT-PCR of mature *IL6* in SCR control and hnRNP M KD cells treated with Pam3CSK4 for 4 h.
(L) Model of cGAS-mediated cytosolic DNA sensing and IFNAR signaling.
(M) qRT-PCR of *Mx1* and *Ifnb* mRNA levels in SCR control and hnRNP M KD cells at 4 h following ISD transfection.
(N) qRT-PCR of ISGs (*Ifit* and *Irf7*) in SCR control and hnRNP M KD cells at 4 h following ISD transfection
(O) qRT-PCR of *Mx1* transcript in SCR control and hnRNP M KD cells treated with recombinant IFN-β for 4 h.
All experiments represent 3 biological replicates where values are means ± SEM, n = 3.

M could specifically influence constitutive intron removal and/or alternative splicing in LPS-activated macrophages. We chose *IL6* as a model transcript because (1) it has a simple intron-exon architecture with four relatively short introns (165, 1,271, 3,059, and 1,226 nucleotides, respectively); (2) it was robustly hyperinduced by loss of hnRNP M (Figures 1F and 1H); and (3) it is a crucial component of the macrophage inflammatory response. Using qRT-PCR, we first measured the relative abundance of each *IL6* intron-exon junction (Figure 3A) in SCR control cells to assess how intron removal proceeded on *IL6* pre-mRNAs in cells containing hnRNP M. Primers were designed to only amplify introns that are still part of pre-mRNAs and not released intron lariats. At 2 h post-LPS treatment, most of the *IL6* transcripts we detected were partially processed, with intron 1 and to some extent intron 4 being preferentially removed and introns 2 and 3 being retained (Figure 3B). We then compared the relative abundance of *IL6* introns in SCR control cells to those in hnRNP M KD macrophages and observed a dramatic and specific decrease in intron 3-containing *IL6* pre-mRNAs in the absence of hnRNP M. This decrease in *IL6* intron 3 starkly contrasted other *IL6* intron-exon and exon-exon junctions, which were overall more abundant in the absence of hnRNP M (Figure 3C). The fact that we observe vastly different amounts of intron 2 and 4-containing *IL6* pre-mRNAs compared to intron-3-containing *IL6* pre-mRNAs in hnRNP M KD macrophages speaks against hnRNP M impacting *IL6* expression transcriptionally and instead argues strongly for the protein playing a role in *IL6* pre-mRNA processing. These data demonstrate that *IL6* pre-mRNAs accumulate in the absence of hnRNP M and suggest that *IL6* intron 3 plays a privileged role in dictating the maturation of *IL6* mRNAs. Specifically, we propose that retention of intron 3 serves as a rate-limiting step in *IL6* pre-mRNA processing so that in the absence of hnRNP M, when *IL6* intron 3 is removed more efficiently, higher levels of mature *IL6* mRNA are made (Figures 1F, 1H, and 2B). Consistent with a role for hnRNP M in controlling splicing specifically, we did not observe any significant differences in the stability of *IL6* mRNAs in hnRNP M KD macrophages compared to SCR controls following a time course of Actinomycin D treatment (Figure S3A).

We next wanted to explore whether loss of hnRNP M also influenced alternative splicing in uninfected and *Salmonella*-infected macrophages. To do so, we employed an algorithm for local splice variation (LSV) analysis called MAJIQ (Modeling Alternative Junction Inclusion Quantification) (Vaquero-Garcia et al., 2016). MAJIQ allows identification, quantification, and visualization of diverse LSVs, including alternative 5′ or 3′ splice site usage and exon skipping, across different experimental conditions. MAJIQ identified a total of 94 LSVs in uninfected SCR versus hnRNP M KD macrophages and 67 LSVs in *Salmonella*-infected SCR versus hnRNP M KD macrophages (probability [|delta PSI|, $\geq$20%], >95%) (Figure 3D). The vast majority of the LSVs identified in SCR versus hnRNP M KD cells were exon skipping events (Figure 3D). Subsequent visualization of these LSVs by Voila analysis revealed that loss of hnRNP M generally correlated with increased exon inclusion in both uninfected and *Salmonella*-infected macrophages. In other words, the presence of hnRNP M led to more exon skipping, which is consistent with a role for hnRNP M in splicing repression. We also conducted IPA pathway analysis of alternatively spliced transcripts to identify pathways enriched for hnRNP M-dependent changes. In contrast to our global gene expression IPA analysis, we observed no enrichment for genes in innate immune-related pathways in either uninfected or *Salmonella*-infected macrophages (Figure 3E). In fact, only 3 transcripts had both significant expression changes (via RNA-seq) and significant delta PSI changes (via MAJIQ), suggesting that hnRNP M's role in influencing steady-state gene expression of innate immune transcripts is distinct from its role in controlling alternative splicing decisions (Figure S3B). Interestingly, the greatest number of splicing changes were induced by *Salmonella* infection itself (Figure S3C), consistent with previously published datasets (Kalam et al., 2017; Pai et al., 2016).

Mx1, an anti-viral GTPase, was one of the three transcripts significantly impacted by loss of hnRNP M at the levels of gene expression (Figures 1F and 1H) and alternative splicing (Figure 3F). Specifically, MAJIQ identified an exon inclusion event of *Mx1* "exon 9" that was significantly more frequent in hnRNP M KD uninfected macrophages versus SCR control uninfected macrophages (delta PSI exon 8-exon 9 = 0.703 versus exon 8-exon 10 = 0.298) (Figure 3G). Inclusion of this exon 9 introduces a premature stop codon and exon-9-containing transcript isoforms of *Mx1* are annotated as nonsense-mediated decay targets. Together with our RNA-seq analysis, these results suggest that the overall abundance of Mx1 protein may be regulated by hnRNP M at multiple post-transcriptional processing steps, i.e., bulk transcript abundance and proportion of functional protein-encoding transcripts. MAJIQ also reported increased exon inclusion events for *Commd8*, a putative transcriptional regulator, and *Nmt2*, an N-myristoyltransferase. We confirmed each of these LSVs by semi-quantitative RT-PCR (Figures 3H, 3I, and S3D). Collectively, these data illustrate that hnRNP M can repress splicing of both constitutive and alternative introns, leading to distinct transcript and protein expression outcomes in macrophages.

hnRNP M Is Enriched at the Level of Chromatin and at the IL6 Genomic Locus

To get a better understanding of how hnRNP M controls pre-mRNA splicing, we next asked where hnRNP M localizes in RAW 264.7 macrophages and whether its localization changed upon TLR4 activation. Other hnRNP family members have been found to translocate to the cytoplasm in response to several different types of stimuli including vesicular stomatitis virus (VSV) infection, osmotic shock, and inhibition of transcription (Allemand et al., 2005; Lichtenstein et al., 2001; Pettit Kneller et al., 2009), and hnRNP U has been shown to shuttle out of the nucleus following LPS treatment of macrophages (Zhao et al., 2012). Based on our data implicating hnRNP M in splicing, we predicted that it can function in the macrophage nucleus and indeed, several algorithms including nuclear localization signal (NLS) Mapper (Kosugi et al., 2009) and PredictProtein (Yachdav et al., 2014) predicted hnRNP M is a predominantly nuclear protein (NLS Mapper score 8.5/10; PredictProtein 98/100) (Figure 4A).

To examine hnRNP M localization, we performed immunofluorescence microscopy in uninfected macrophages using an

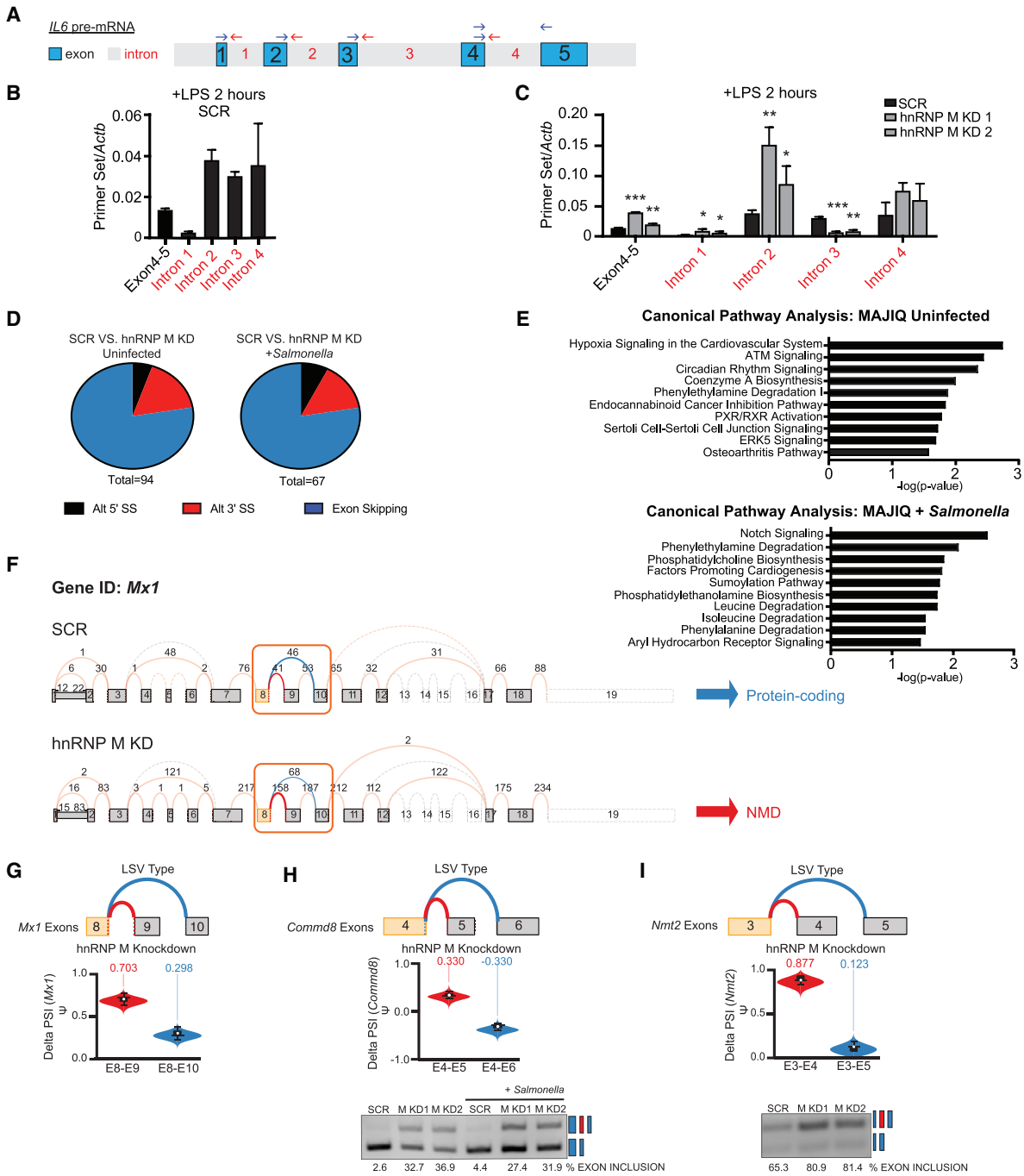

Figure 3. hnRNP M Influences Gene Expression Outcomes at the Level of Pre-mRNA Splicing

(A) Diagram of *IL6* pre-mRNA with introns (gray) and exons (blue).

(B) qRT-PCR of *IL6* exon-exon and intron-exon junctions in SCR control macrophages at 2 h post-LPS treatment.

(C) qRT-PCR of *IL6* exon-exon and intron-exon junctions in SCR versus hnRNP M KD1 and KD2 at 2 h post-LPS treatment.

(D) Categorization of alternative splicing events identified via MAJIQ in uninfected SCR versus hnRNP M KD1 samples and in *Salmonella*-infected SCR versus hnRNP M KD1 samples.

(E) Ingenuity Pathway Analysis of hnRNP M-dependent genes from MAJIQ analysis in uninfected and *Salmonella*-infected cells.

(F) VOILA output of *Mx1* transcript model in SCR and hnRNP M KD1 cells infected with *Salmonella*.

(G) Violin plots depicting the delta PSI of hnRNP M-dependent local splicing variations in *Mx1*.

(H) As in (G) but for *Commd8*, alongside semiquantitative RT-PCR validation.

(I) As in (H) but for *Nmt2*.

(B) and (C) are representative of two independent experiments that showed the same result with values representing means (SD), n = 3.

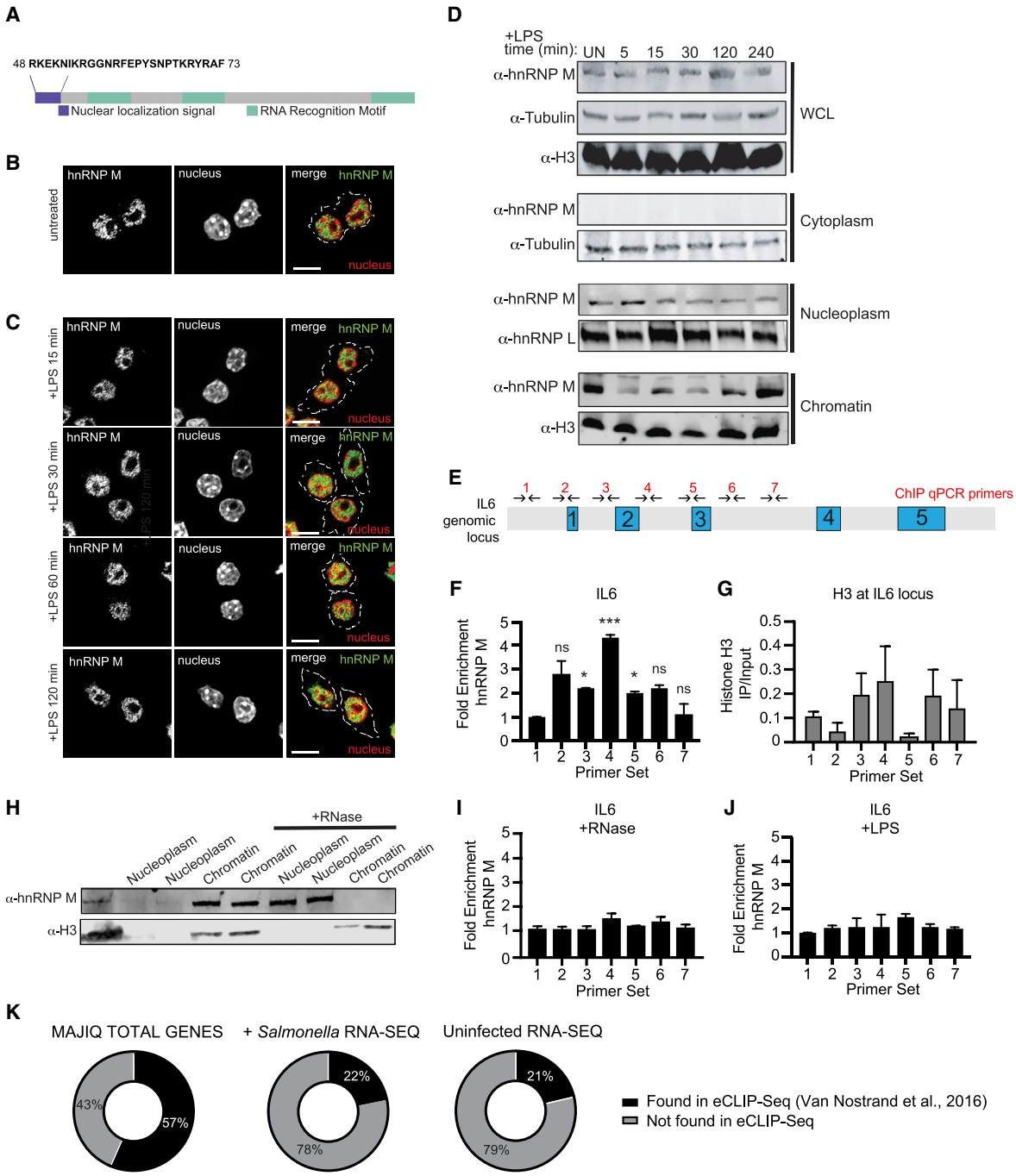

Figure 4. hnRNP M Is a Nuclear Protein that Associates with the IL6 Genomic Locus in an RNA-Dependent Fashion

(A) Schematic diagram of hnRNP M, highlighting the nuclear localization signal (purple) and three RNA Recognition Motifs (green).

(B) Immunofluorescence images of uninfected RAW 264.7 macrophages immunostained with anti-hnRNP M (green).

(C) Immunofluorescence images of RAW 264.7 macrophages stimulated with LPS for the respective time points and immunostained with anti-hnRNP M (green). Scale bar, 10 μM.

(D) Western blot analysis of cellular fractions with anti-hnRNP M and loading controls of cytoplasm (tubulin), nucleoplasm (hnRNP L) and chromatin (H3) fractions of uninfected and LPS stimulated RAW 264.7 macrophages.

(E) ChIP-qPCR primers designed to tile the IL-6 locus.

(F) qPCR of ChIP at the *IL6* genomic locus with anti-hnRNP M in resting RAW 264.7 macrophages.

(G) As in (F) but using an anti-histone H3 antibody.

(H) Western blot analysis of nuclear and chromatin fractions with anti-hnRNP M and Histone H3 (control) with untreated and RNase-treated nuclear fractions.

(legend continued on next page)

anti-hnRNP M antibody and observed significant nuclear enrichment (Figure 4B) with no major changes over a 2 h time course of LPS treatment (Figure 4C). This was true for endogenous hnRNP M and a 3xFLAG-hnRNP M allele stably expressed in macrophages (Figure S4A). As a control, we monitored the translocation of hnRNP U upon LPS treatment and observed nuclear to cytoplasmic translocation, consistent with previous reports (Figure S4B). Based on these results, we concluded that hnRNP M is a nuclear protein in macrophages and that LPS treatment does not trigger translocation to another cellular compartment.

We next sought to understand more precisely where in the nucleus hnRNP M was enriched since intron recognition and removal can occur at the level of chromatin, while nascent transcripts are still tethered to RNA polymerase II (Bhatt et al., 2012; Moehle et al., 2014; Nojima et al., 2016; Pandya-Jones and Black, 2009). To this end, we performed a cellular fractionation experiment in RAW 264.7 macrophages over a time course of LPS treatment and visualized hnRNP M localization via western blot (Figure 4D). We observed hnRNP M in both the nucleoplasm and the chromatin over the course of LPS treatment, while no hnRNP M was detectable in the cytoplasmic fraction. Macrophages stably expressing 3xFLAG-hnRNP M showed a similar hnRNP M distribution between the nucleoplasm and chromatin (Figure S4C). We did not observe significant redistribution of either endogenous or 3xFLAG-hnRNP M between the nucleoplasm and chromatin fractions upon LPS treatment (Figures 4D and S4C). Residual hnRNP M protein expressed in KD cell lines was similarly distributed between the chromatin and nucleoplasm (Figure S4D). Together, fractionation and immunofluorescence experiments confirmed that a population of hnRNP M associates with chromatin, and the protein does not grossly redistribute in the cell upon LPS treatment.

hnRNP M's Association with the IL6 Locus Is RNA Dependent and Controlled by TLR4 Signaling

We next wanted to determine whether hnRNP M's association with chromatin was specific for the genomic loci of genes whose regulation was impacted by hnRNP M (Figure 1F). We hypothesized that, if hnRNP M repression of *IL6* intron 3 removal occurs at the nascent transcript level, then hnRNP M may associate with the IL6 genomic locus. To test this, we performed chromatin immunoprecipitation (ChIP)-qPCR. ChIP has been used extensively in yeast and to some extent in mammals as a spatiotemporal read out of splicing factor recruitment to nascent transcripts (Bieberstein et al., 2014; Moehle et al., 2012; Neves et al., 2017; Nissen et al., 2017; Patrick et al., 2015). Endogenous hnRNP M was immunoprecipitated from untreated macrophages, and association with the IL6 locus (DNA) was determined using a series of tiling primers spaced approximately 500 bp apart (Figure 4E). We observed no enrichment of hnRNP M in the promoter region of IL6, consistent with it playing a mainly post-transcriptional role in *IL6* processing (Figure 4F, primer set 1). We did, however, observe significant enrichment of hnRNP M at several primer sets in the IL6 gene, most notably over the intron 2-intron 3 region (Figure 4F, primer sets 3–5). Previously published cross-linking immunoprecipitation (CLIP)-seq experiments identified a GUGGUGG consensus site for hnRNP M (Huelga et al., 2012); such a site exists in intron 2 of *IL6,* and several similar motifs are found in *IL6* intron 3 (Figure S4E). Indeed, of all the transcripts in Figure 1D, >75% of them contain at least one consensus hnRNP M motif in an intron (Table S2). ChIP-qPCR of histone H3, which showed clear depletion of nucleosomes around the IL6 transcription start site (primer sets 1 and 2), was performed to control for genomic DNA accessibility and/or primer set efficiency (Figure 4G). Together, these results reveal that hnRNP M can associate with the genomic locus of transcripts like *IL6* whose splicing it represses, suggesting that it functions co-transcriptionally. Importantly, treatment with RNase A shifted hnRNP M from the chromatin into the nucleoplasm (Figure 4H). Likewise, RNase A treatment (Bieberstein et al., 2014) abolished hnRNP M enrichment at the IL6 genomic locus via ChIP-qPCR as well, confirming that its association with chromatin and the IL6 gene depends on RNA (Figure 4I).

If hnRNP M acts as a repressor of *IL6* splicing by binding to nascent transcripts at the IL6 locus, we hypothesized that this repression might be relieved upon TLR4 activation, thus allowing a cell to robustly induce IL-6 expression following pathogen sensing. To test this, we performed ChIP-qPCR of hnRNP M at the IL6 locus in RAW 264.7 macrophages treated with LPS for 1 h. Remarkably, we observed a complete loss of hnRNP M enrichment at all primer sets along the IL6 gene body, including those over intron 2 and 3, following LPS treatment (Figure 4J). This result strongly links hnRNP M's ability to repress *IL6* with its presence at the IL6 genomic locus and suggests that TLR4 signaling controls hnRNP M's repressor activity.

Having demonstrated that hnRNP M's ability to associate with the IL6 chromatin locus relies on RNA, we were curious to see whether hnRNP M directly binds to transcripts whose expression were hnRNP M dependent (Figures 1C and 1D). To begin to answer this question, we leveraged previously published datasets of hnRNP M-bound transcripts in two human cell lines HepG2 (human liver carcinoma cells) and K562 (human chronic myelogenous leukemia cells) (Van Nostrand et al., 2016). Remarkably, we observed almost 60% overlap between our MAJIQ genes and the enhanced CLIP (eCLIP) datasets (Figure 4K; Table S3), suggesting that hnRNP M's alternative splicing targets are highly conserved between mouse and human and that the transcripts identified in our MAJIQ analysis are direct hnRNP M targets. While the overlap between the eCLIP hits and differentially expressed transcripts from our RNA-seq analysis (RNA-seq hits, Figures 1C and 1D) was lower (22% for *Salmonella*-infected transcripts, 21% for uninfected transcripts), this result is not altogether surprising, as HepG2 cells

(I) As in (F) but with 30 min incubation at 37° with RNase A.
(J) As in (F) but with macrophages treated with 100 ng/mL LPS for 1 h.
(K) Venn diagrams representing hnRNP M eCLIP (ENCODE) gene overlap with our MAJIQ, uninfected RNA-seq, and *Salmonella*-infected RNA-seq results.
(F) and (G) values are means ± SEM representative of 2 biological replicates, n = 2. (I) and (J) values are means ± SEM representative of 3 biological replicates, n = 3.

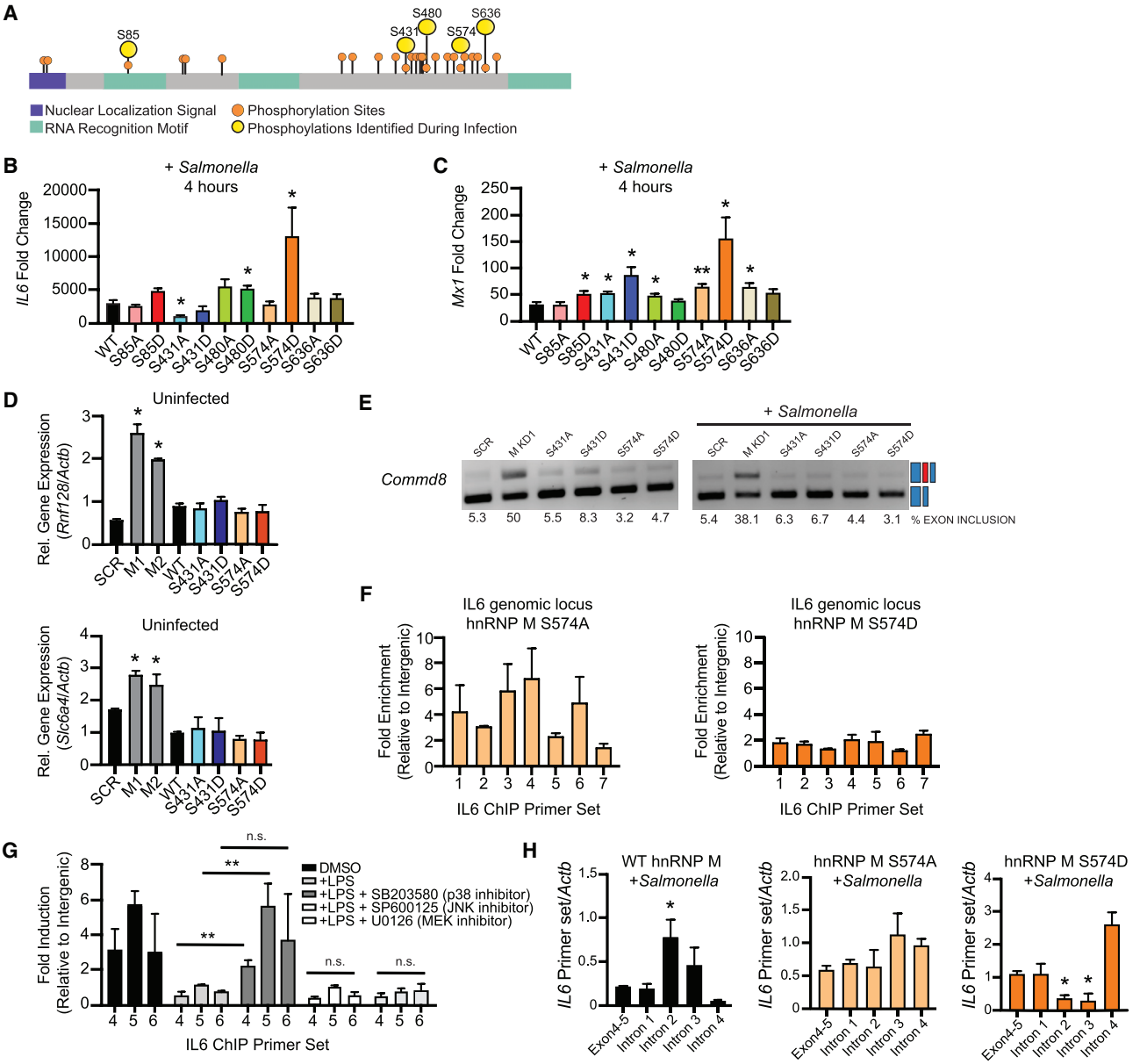

Figure 5. Phosphorylation of hnRNP M at S574 Downstream of TLR4 Activation Controls Its Ability to Repress Expression of Innate Immune Transcripts

(A) Protein diagram of hnRNP M indicating location of phosphorylation sites identified by SILAC/mass spectrometry (Penn et al., 2018) with nuclear localization signal shown in purple and RNA-recognition motifs (RRM) shown in in green.

(B) qRT-PCR of mature *IL6* in wild-type (WT) hnRNP M-FLAG and phosphomutants in macrophages infected with *Salmonella* for 4 h.

(C) As in (B) but for *Mx1*.

(D) qRT-PCR of *Rnf128* and *Slc6a4* in uninfected, WT 3xFL-hnRNP M, and phosphomutants.

(E) Semiquantitative PCR of *Commd8* alternative splicing in cells expressing SCR or hnRNP M KD constructs alongside phosphomutant-expressing alleles.

(F) ChIP-qPCR of hnRNP M-S574A/D alleles at the *IL6* genomic locus.

(G) ChIP-qPCR of wild-type 3xFL-hnRNP M in the presence of 100 ng/mL LPS and various MAPK inhibitors (SB203580, SP600125, and U0126).

(H) RT-qPCR of *IL6* intron-exon junctions and the exon 4–5 mature junction in 3xFL-hnRNP M and 3xFL-hnRNP M 574A and 574D phosphomutants, in macrophages infected with *Salmonella* for 4 h.

(B)–(D) are representative of 3 biological replicates with values indicating means ± SEM, n = 3. (F)–(H) are representative of 2 biological replicates values indicating means ± SEM, n = 2. (I) is representative of 2 independent experiments that showed the same result with values representing means (SD), n = 3.

and K562 cells would not be expected to express many of the same transcripts as a macrophage. However, together these data reinforce the idea that RBPs like hnRNP M can play specialized roles in different cellular contexts, while also regulating a core set of conserved target transcripts.

Phosphorylation of hnRNP M at S574 Downstream of TLR4 Activation Controls Its Ability to Repress Expression of Innate Immune Transcripts

A recently published phosphoproteomics dataset identified a number of splicing factors that were differentially phosphorylated during infection with the intracellular bacterium *Mycobacterium tuberculosis* (Penn et al., 2018). Because it is not a gram-negative bacterium, *M. tuberculosis* does not activate TLR4 via LPS, but it does express the lipoglycan lipomannan (LM) and other lipoproteins, which are agonists of TLR2. Having confirmed hnRNP M-dependent regulation of *IL6* following treatment with a TLR2 agonist (Pam3CSK4) (Figure 2K), we reasoned that TLR2 activation upon *M. tuberculosis* infection may lead to the same changes in hnRNP M phosphorylation as would TLR4 activation during *Salmonella* infection. We thus leveraged the *M. tuberculosis* global phosphoproteomics dataset from Penn et al. (2018), identified 5 differentially phosphorylated serine residues on hnRNP M (S85, S431, S480, S574, and S636) (Figure 5A), and generated 3xFLAG-hnRNP M constructs with phosphomimic (S → D) or phosphodead (S → A) mutations at each of the serines and made stable RAW 264.7 macrophages expressing each of these alleles in wild-type RAW 264.7 macrophages that still contain a wild-type hnRNP M allele. Importantly, we did not observe any significant differences in the expression level of these mutant alleles compared to the wild-type 3xFLAG-hnRNP M either in resting macrophages or over a course of LPS treatment (Figure S5A).

Although the phosphoproteomics dataset predicts infection-dependent gain of phosphorylation at some sites and loss of phosphorylation at others, we were curious as to whether we could detect bulk hnRNP M phosphorylation changes via western blot analysis. While we were unable to detect any higher- or lower-molecular-weight species using antibodies against the endogenous protein, we consistently measured accumulation of a higher-molecular-weight species of the wild-type 3xFLAG-hnRNP M allele over the course of LPS treatment, with an initial increase in the species seen as early as 15 min post-treatment (Figure S5B), consistent with a population of hnRNP M being post-translationally modified upon pathogen sensing.

To determine how these individual serine residues contribute to hnRNP M activity during macrophage activation, we infected each of the phosphomutant/mimic-expressing cell lines, as well as a control expressing a wild-type allele, with *Salmonella* and measured *IL6* and *Mx1* expression at 4 h. Remarkably, expression of hnRNP M harboring a single serine mutation (hnRNP M 574D) caused dramatic hyperinduction of both *IL6* and *Mx1* compared to cells expressing the wild-type 3xFLAG-hnRNP M allele (Figures 5B and 5C). Several other phosphomutant alleles (S85D, red bar, S431A, light-blue bar, S480A/D, green bars) also affected *IL6* and *Mx1* induction but to a lesser extent (Figures 5B and 5C). Mutating S587, which is a repeat of the S574-containing sequence (MGANS(ph)LER), did not affect the regulation of *IL6* or *Mx1*, suggesting the location of these serines is critical and that phosphorylation-dependent regulation of hnRNP M is specific for select serine residues (Figure S5C). Curiously, expression of the S574D allele in the hnRNP M KD cell lines did not recapitulate this derepression phenotype, suggesting the 574D allele disrupts the activity of wild-type hnRNP M itself—perhaps via interfering with hnRNP M protein oligomerization and/or higher-order complexes that form at innate immune targets (Figure S5D).

Having implicated hnRNP M phosphorylation at S574 in controlling *IL6* and *Mx1* expression, we next wanted to see how phosphorylation affected transcripts whose expression in uninfected cells was higher in the absence of hnRNP M (Figure 1G). While we again observed elevated expression of these transcripts in the absence of hnRNP M (hnRNP M KD, gray bars), expression of the phosphomutant alleles (S431A/D and S574A/D) had no effect on *Rnf128*, *Rnf26*, or *Slc6a4* transcript levels (Figure 5D). Expression of these genes was similarly unaffected by the other hnRNP M phosphomutants (Figure S5E). Alternative splicing of *Commd8* was also unaffected by any of the phophosmutants in either uninfected or *Salmonella*-infected cells (Figure 5E). Together, these data provide strong evidence that hnRNP M's ability to regulate the expression of constitutively expressed genes and/or influence alternative splicing decisions does not rely on phosphorylation at serine 574, whereas its role in regulating innate immune transcripts induced during infection is specifically controlled by PTMs downstream of pathogen sensing.

Like wild-type hnRNP M, each hnRNP M phosphomutant was enriched in the chromatin in untreated cells (Figure S5F). However, in ChIP experiments looking specifically at the IL6 locus, the S574D phosphomimic allele displayed virtually no enrichment compared to the S574A phosphodead allele, whose enrichment profile was similar to that of wild-type hnRNP M (Figure 5F and Figure 4F). Indeed, hnRNP M 574D ChIPs more closely resembled those from RNase- or LPS-treated samples (Figures 4I and 4J). These data point to phosphorylation of residue S574 in controlling hnRNP M's ability to co-transcriptionally repress processing of chromatin-associated *IL6* pre-mRNAs.

We next sought to better understand how hnRNP M is phosphorylated at these key residues. TLR4 activation triggers a number of signaling cascades, including p38, MEK1/2 (ERK), and JNK MAP kinases. Previous reports have implicated each of these pathways in regulating *IL6* expression downstream of innate immune stimuli (Costa-Pereira, 2014), but it is not known whether these cascades control splicing factor phosphorylation. To test the role of each cascade in hnRNP M-dependent repression of *IL6*, we performed ChIP experiments in the presence of LPS and specific inhibitors of p38 (SB203580), JNK (SP600125), or MEK (U0126). We again observed LPS-dependent loss of hnRNP M enrichment at IL6 (primer sets 4–6), and treatment with JNK and MEK inhibitors had no effect on hnRNP M release. However, in the presence of the p38 inhibitor, hnRNP M remained associated with the IL6 genomic locus after LPS treatment (Figure 5G), demonstrating that p38 signaling promotes release of hnRNP M from the IL-6 genomic locus.

Last, to interrogate the mechanism driving *IL6* hyperinduction in hnRNP M S574D-expressing cells, we asked whether *IL6*

intron removal was affected by expression of the phosphomutant alleles. Using the same qRT-PCR approach used in Figure 3B, we detected an increase in *IL6* pre-mRNAs containing introns 2 and 3 in macrophages overexpressing a wild-type hnRNP M allele, consistent with hnRNP M slowing *IL6* intron removal. Conversely, these same introns were removed more efficiently in the presence of hnRNP M S574D, while no difference was observed in S574A-expressing cells (Figure 5H). These data strongly support a model whereby phosphorylation of hnRNP M at S574 relieves its ability to act as a splicing repressor, allowing for rapid removal of *IL6* introns and upregulation of *IL6* mRNA, and demonstrate a previously unappreciated role for constitutive intron removal in mediating *IL6* expression in macrophages.

Loss of hnRNP M Enhances Macrophages' Ability to Control Viral Infection

Because loss of hnRNP M resulted in hyperinduction of a variety of cell-intrinsic antimicrobial molecules and ISGs, we hypothesized that hnRNP M KD cells would be better at controlling viral replication. We infected SCR and hnRNP M KD RAW 264.7 macrophages with VSV, an enveloped RNA virus that can replicate and elicit robust gene expression changes in RAW 264.7 macrophages (Kandasamy et al., 2016). Viral replication (levels of VSV-G) was measured over an 8 h time course by qRT-PCR in cells infected with a viral MOI of 1 and 0.1. At both MOIs, loss of hnRNP M correlated with dramatic restriction of VSV replication, particularly at the 8 h time point (Figure 6A). As expected, infection with VSV, a potent activator of cytosolic RNA sensing via RIG-I/MAVS (Kandasamy et al., 2016), led to robust induction of *Ifnb* levels in an hnRNP M-independent fashion at both MOIs, as we previously observed in hnRNP M KD cells transfected with cytosolic dsDNA (Figures 6B, S6A, and 2M, respectively). Consistent with hnRNP M-dependent regulation occurring downstream of diverse immune stimuli (Figure 2), VSV-infected hnRNP M KD cells at MOI = 1 and MOI = 0.1 hyperinduced both *Mx1* and *IL6* (Figures 6C, 6D, S6B, and S6C).

While *Mx1* itself is a well-known anti-viral GTPase, cell lines derived from inbred mouse strains like RAW 264.7 have been shown to carry non-functional *Mx1* alleles (Shin et al., 2015). Therefore, to begin to predict what other hnRNP M-regulated genes may be responsible for enhanced VSV restriction, we manually examined hnRNP M-regulated transcripts in our RNA-seq data from uninfected and *Salmonella*-infected (i.e., TLR4-activated) macrophages and identified a number of genes known to be important for controlling RNA viral replication (Figure 6E). qRT-PCR confirmed hyperinduction of several antiviral ISGs in hnRNP M KD macrophages at 4 h post-VSV infection including *Rsad2* (Viperin), *Ifit1*, *Irf7*, and *Gbp5* (Figure 6F). Interestingly, neither *Ifit1* nor *Irf7* was identified as an hnRNP M-dependent transcript during *Salmonella* infection, even though both can be expressed downstream of TLR4 through IRF3/IFNAR/STAT1 signaling. This difference may simply reflect kinetic differences in transcript induction following RNA sensing versus TLR4 activation or may indicate that hnRNP M regulates an even broader set of transcripts in macrophages following RNA virus infection. We propose that inhibition of VSV replication in hnRNP M KD macrophages ultimately results from a combination of pro-viral gene downregulation (red genes, Figure 6E) and anti-viral gene upregulation (blue genes, Figure 6E and Figure 6F). Collectively, these data are consistent with hnRNP M playing a critical role in slowing innate immune gene expression and suggest that the presence of hnRNP M can actually blunt macrophage antiviral defenses at early time points following infection with VSV.

DISCUSSION

Despite the substantial impact pre-mRNA splicing has on gene expression outcomes, little is known about how components of the spliceosome are modified and regulated during cellular reprogramming events, such as macrophage pathogen sensing. Here, we demonstrate that the splicing factor hnRNP M is a critical repressor of a unique regulon of innate immune transcripts (see model in Figure 7). These transcripts were hyperinduced in hnRNP M KD macrophages downstream of a variety of innate immune stimuli (i.e., *Salmonella* infection, TLR4/TLR2 agonists, recombinant IFN-β, cytosolic dsDNA, RNA virus infection [VSV]) (Figure 2; Figure 6), and hyperinduction of this regulon correlated with enhanced capacity of hnRNP M KD macrophages to control VSV replication at early time points (Figure 6). We propose that in innate immune cells like macrophages repression of pre-mRNA splicing by hnRNP M serves as a safeguard, dampening the initial ramping up of innate immune gene expression and preventing spurious expression of potent pro-inflammatory molecules in situations where the cell has not fully engaged with a pathogen. The latter situation is supported by experiments in which low doses of LPS (10 and 50 ng/mL), were sufficient to hyperinduce *IL6* in the absence of hnRNP M without inducing significant a change in the amount of *IL6* mRNA expressed in SCR control cells (Figure S7A). These data support a role for hnRNP M in slowing *IL6* processing in macrophages that are "sampling" PAMPs or that have just received an initial innate immune stimulus. The requirement for cells to tightly control expression of potent inflammatory mediators like *IL6* is evidenced by the fact that multiple transcriptional and post-transcriptional mechanisms exist to regulate *IL6*, including chromatin remodeling (Ramirez-Carrozzi et al., 2009), mRNA stability (Masuda et al., 2013), subcellular localization (Higa et al., 2018), and now, based on these data, pre-mRNA splicing. While hnRNP M's role in regulating many alternative splicing decisions is conserved across diverse cell types in mice and humans (as evidenced by overlap in our MAJIQ hits and eCLIP datasets [Figure 4K]), its role in controlling innate immune transcripts is uniquely influenced by phosphorylation downstream of pathogen sensing. Based on these observations, we propose that hnRNP M and likely other splicing factors possess distinct capacities for interacting with RNAs and/or proteins depending on how they are post-translationally modified. In this way, innate immune sensing cascades may remodel splicing complexes, for example, by promoting release of hnRNP M from chromatin-associated RNA-proteins complexes via p38-MAPK cascades.

While we do not fully understand the mechanisms driving hnRNP M's target specificity, our RNA-seq data as well as other datasets (Bhatt et al., 2012) demonstrate the presence of cryptic exons in a number of hnRNP M-regulated transcripts (Figure S7). Previous work investigating the

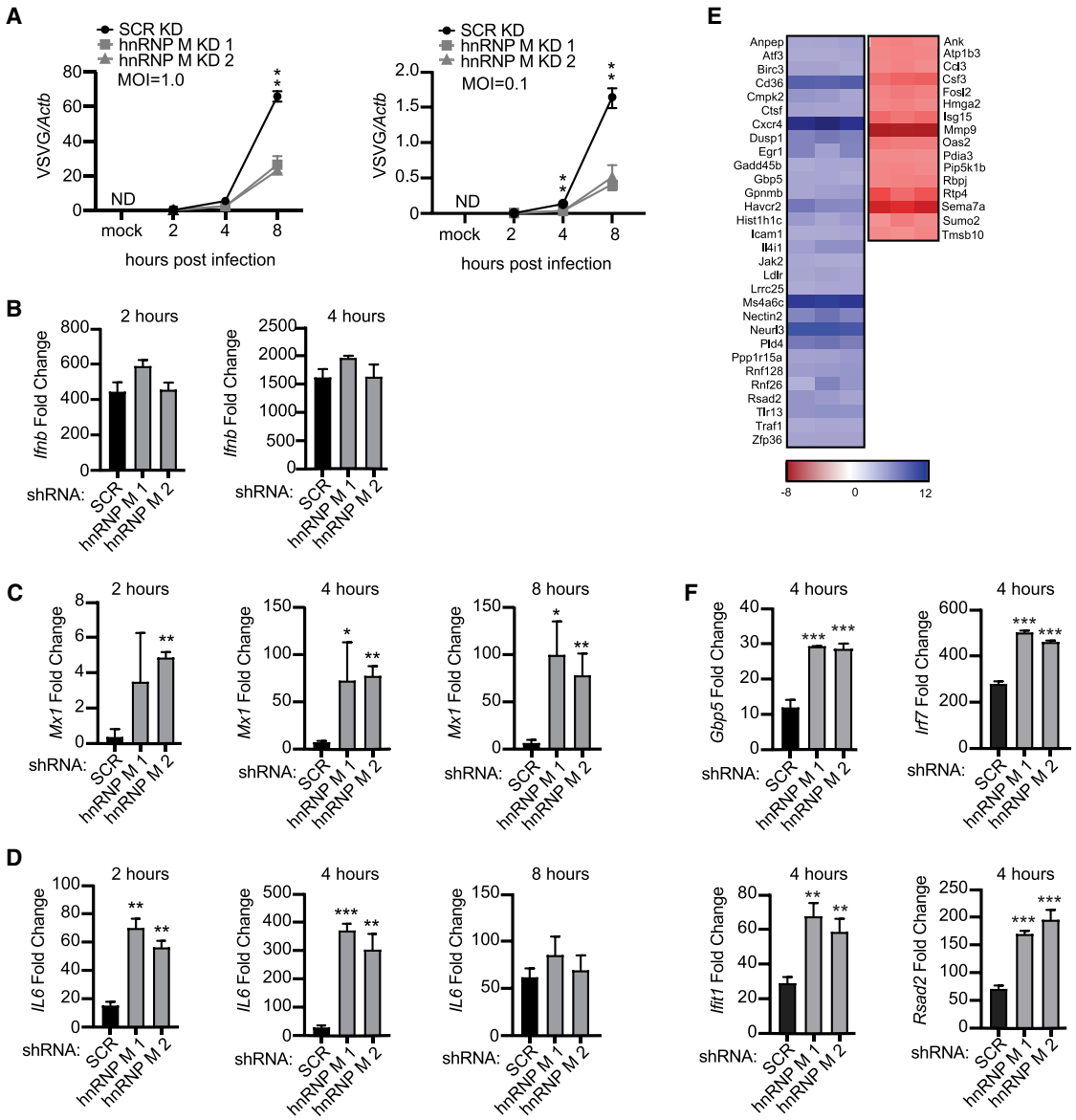

Figure 6. Knockdown of hnRNP M Enhances a Macrophage's Ability to Control Viral Infection

(A) Viral replication in hnRNP M KD and SCR control RAW 264.7 macrophages infected with VSV (MOI = 1.0, MOI = 0.1, or Mock) at 2, 4, and 8 h post-infection.

(B) qRT-PCR of *Ifnb* mRNA levels in SCR control and hnRNP M KD cells at 2 and 4 h post-infection, MOI = 1.

(C) qRT-PCR of *Mx1* transcript in VSV-infected SCR control and hnRNP M KD cells at 2, 4, and 8 h post-infection, MOI = 1.

(D) qRT-PCR of *IL6* transcript in SCR control and hnRNP M KD cells at 2, 4, and 8 h post-infection MOI = 1.

(E) Differential gene expression in hnRNP M KD cells compared to SCR control macrophages from earlier RNA-seq analysis (Figure 1) highlighting known viral response genes.

(F) qRT-PCR of *Ifit*, *Irf7*, *Rsad2*, and *Gbp5* mRNA levels in SCR control and hnRNP M KD cells at 4 h post-infection, MOI = 1.

(A)–(E) are representative of 2 biological replicates with values indicating means ± SEM, n = 2. (F) is representative of 2 independent experiments that showed the same result with values representing means (SD), n = 3.

RNA-binding landscape of a panel of hnRNP proteins in a non-macrophage cell line (HEK293Ts, human embryonic kidney cells) revealed that hnRNP M has a strong preference for binding distal intronic regions (>2 kb from an exon-intron junction) (Huelga et al., 2012). Its binding profile was somewhat unique among the hnRNPs queried and was more reminiscent of another RBP, TDP-43. TDP-43 also binds UG-rich sites in distal introns and is crucial for repressing splicing of cryptic exons for a set of transcripts in the brain (Ling et al., 2016; 2015). We speculate that hnRNP M regulates splicing of macrophage transcripts through a similar mechanism where it binds to UG-rich regions downstream of cryptic exons and inhibits assembly of the spliceosome on these introns, thus slowing intron removal.

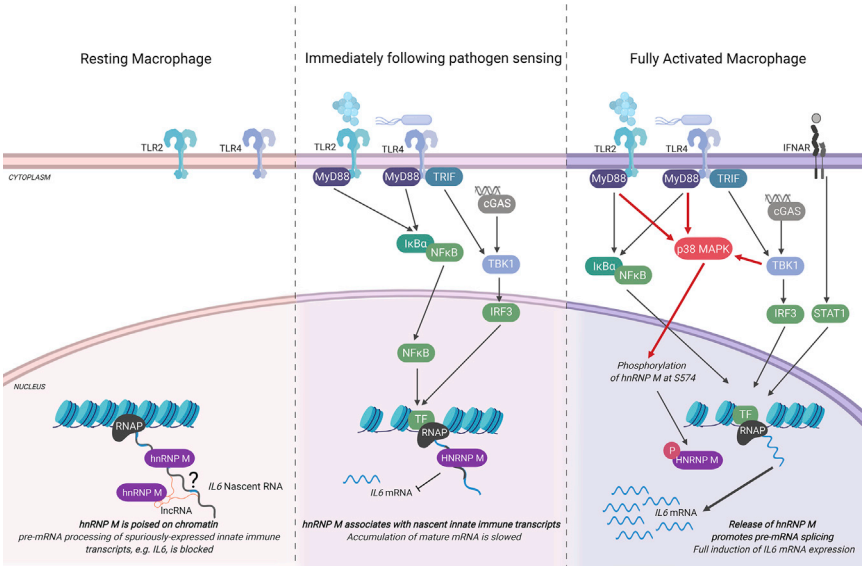

Figure 7. Proposed Model for hnRNP M-Dependent Repression for *IL6* Expression in Resting, Early-, and Late-Activated Macrophages

(Left) In resting macrophages, hnRNP M associates with chromatin, at the IL6 genomic locus, through interactions with RNA. These interactions may be direct with target transcripts expressed at low levels or spuriously or indirect via protein interactions with other RNA binding proteins or through interactions with other chromatin-associated RNAs, e.g., lincRNAs. (Middle panel) When macrophages receive an innate immune stimulus, they transcriptionally activate genes like IL6. A population of "poised" hnRNP M can associate with chromatin-bound pre-mRNAs in these cells, slowing *IL6* intron removal and preventing full maturation of *IL6* nascent transcripts. (Right) As early macrophage activation proceeds, hnRNP M is phosphorylated at S574 in a p38-MAPK-dependent fashion. Phosphorylation of hnRNP M releases it from the IL6 genomic locus, relieves inhibition of *IL6* splicing, and allows for full induction of *IL6* gene expression. Figure generated using BioRender software.

While hnRNP M's ability to associate with the IL6 genomic locus via ChIP is RNA dependent, it is conceivable that hnRNP M controls innate immune gene expression through mechanisms that are independent of direct contacts between hnRNP M and regulated transcripts. Because a number of splicing factors have been shown to impact histone markers and chromatin remodeling, it is possible that hnRNP M promotes epigenetic changes at specific target transcripts (de Almeida et al., 2011; Kim et al., 2011; Martins et al., 2011; Saldi et al., 2016). hnRNP M may also interact with one or more long non-coding RNAs (lncRNAs), a number of which are regulated by TLR activation (Carpenter et al., 2013) and have been shown to control *IL6* expression (Atianand et al., 2016; Carpenter et al., 2013). Experiments designed to identify hnRNP M-associated RNAs in uninfected and infected macrophages will provide important insights into how hnRNP M recognizes chromatin-associated target transcripts and help illuminate how pre-mRNA splicing decisions shape the innate immune transcriptome.

STAR★METHODS

Detailed methods are provided in the online version of this paper and include the following:

- KEY RESOURCES TABLE
- LEAD CONTACT AND MATERIALS AVAILABILITY
- EXPERIMENTAL MODEL AND SUBJECT DETAILS
  - Cell lines
  - Bacterial strains
  - Viral strain
- METHOD DETAILS
  - RNA-SEQ
  - S. Typhimurium Infection
  - LPS Treatment
  - Immunofluorescence Microscopy
  - Western Blots
  - siRNA Transfection
  - Antibodies
  - Cellular fractionation
  - RNase Fractionation
  - Gene Ontology (GO) Canonical Pathway Analysis
  - RNA isolation and qPCR analysis
  - Chromatin Immunoprecipitation
  - FLAG Chromatin Immunoprecipitation
  - Alternative Splicing Analysis
  - VSV infection
- QUANTITATION AND STATISTICAL ANALYSIS
- DATA AND CODE AVAILABILITY

SUPPLEMENTAL INFORMATION

Supplemental Information can be found online at https://doi.org/10.1016/j.celrep.2019.09.078.

ACKNOWLEDGMENTS

We would like to thank Drs. Jeffery Cox, Bennett Penn, and Jonathan Budzik for sharing *M. tuberculosis* phosphoproteomics data and members of the Watson and Patrick labs for critical reading of the manuscript and invaluable feedback. We would also like to thank the Texas A&M AgriLife Genomics & Bioinformatics Services for performing RNA sequencing experiments and providing computing resources. This work was funded by R01AI25512 (R.O.W.) and R21AI4004 (R.O.W. and K.L.P.). A.P.W. and S.T.-O. were supported by the Office of the Assistant Secretary of Defense for Health Affairs through the Peer Reviewed Medical Research Programs under award number W81XWH-17-1-0052. Opinions, interpretations, conclusions, and recommendations are those of the author and are not necessarily endorsed by the Department of Defense.

AUTHOR CONTRIBUTIONS

K.O.W., K.L.P., and R.O.W. designed the project. K.O.W. performed experiments and analyzed data. H.M.S. performed exon-inclusion PCR assays. S.T.-O. and A.P.W. performed VSV infections. K.O.W., K.L.P., and R.O.W.

wrote the paper and created figures. All authors read and approved the final version of the manuscript.

DECLARATION OF INTERESTS

The authors declare no competing interests.

Received: May 3, 2019
Revised: August 13, 2019
Accepted: September 26, 2019
Published: November 5, 2019

REFERENCES

Allemand, E., Guil, S., Myers, M., Moscat, J., Cáceres, J.F., and Krainer, A.R. (2005). Regulation of heterogenous nuclear ribonucleoprotein A1 transport by phosphorylation in cells stressed by osmotic shock. Proc. Natl. Acad. Sci. USA *102*, 3605–3610.

Atianand, M.K., Hu, W., Satpathy, A.T., Shen, Y., Ricci, E.P., Alvarez-Dominguez, J.R., Bhatta, A., Schattgen, S.A., McGowan, J.D., Blin, J., et al. (2016). A Long Noncoding RNA lincRNA-EPS Acts as a Transcriptional Brake to Restrain Inflammation. Cell *165*, 1672–1685.

Bhatt, D.M., Pandya-Jones, A., Tong, A.-J., Barozzi, I., Lissner, M.M., Natoli, G., Black, D.L., and Smale, S.T. (2012). Transcript dynamics of proinflammatory genes revealed by sequence analysis of subcellular RNA fractions. Cell *150*, 279–290.

Bieberstein, N.I., Straube, K., and Neugebauer, K.M. (2014). Chromatin immunoprecipitation approaches to determine co-transcriptional nature of splicing. Methods Mol. Biol. *1126*, 315–323.

Carpenter, S., Aiello, D., Atianand, M.K., Ricci, E.P., Gandhi, P., Hall, L.L., Byron, M., Monks, B., Henry-Bezy, M., Lawrence, J.B., et al. (2013). A long noncoding RNA mediates both activation and repression of immune response genes. Science *341*, 789–792.

Chen, Y.-L., Jiang, Y.-W., Su, Y.-L., Lee, S.-C., Chang, M.-S., and Chang, C.-J. (2013). Transcriptional regulation of tristetraprolin by NF-κB signaling in LPS-stimulated macrophages. Mol. Biol. Rep. *40*, 2867–2877.

Chen, S., Zhang, J., Duan, L., Zhang, Y., Li, C., Liu, D., Ouyang, C., Lu, F., and Liu, X. (2014). Identification of HnRNP M as a novel biomarker for colorectal carcinoma by quantitative proteomics. Am. J. Physiol. Gastrointest. Liver Physiol. *306*, G394–G403.

Chen, W.-Y., Lin, C.-L., Chuang, J.-H., Chiu, F.-Y., Sun, Y.-Y., Liang, M.-C., and Lin, Y. (2017). Heterogeneous nuclear ribonucleoprotein M associates with mTORC2 and regulates muscle differentiation. Sci. Rep. *7*, 41159.

Cho, S., Moon, H., Loh, T.J., Oh, H.K., Cho, S., Choy, H.E., Song, W.K., Chun, J.-S., Zheng, X., and Shen, H. (2014). hnRNP M facilitates exon 7 inclusion of SMN2 pre-mRNA in spinal muscular atrophy by targeting an enhancer on exon 7. Biochim. Biophys. Acta *1839*, 306–315.

Cobianchi, F., Calvio, C., Stoppini, M., Buvoli, M., and Riva, S. (1993). Phosphorylation of human hnRNP protein A1 abrogates in vitro strand annealing activity. Nucleic Acids Res. *21*, 949–955.

Costa-Pereira, A.P. (2014). Regulation of IL-6-type cytokine responses by MAPKs. Biochem. Soc. Trans. *42*, 59–62.

Dalton, K.P., and Rose, J.K. (2001). Vesicular stomatitis virus glycoprotein containing the entire green fluorescent protein on its cytoplasmic domain is incorporated efficiently into virus particles. Virology *279*, 414–421.

de Almeida, S.F., Grosso, A.R., Koch, F., Fenouil, R., Carvalho, S., Andrade, J., Levezinho, H., Gut, M., Eick, D., Gut, I., et al. (2011). Splicing enhances recruitment of methyltransferase HYPB/Setd2 and methylation of histone H3 Lys36. Nat. Struct. Mol. Biol. *18*, 977–983.

De Arras, L., and Alper, S. (2013). Limiting of the innate immune response by SF3A-dependent control of MyD88 alternative mRNA splicing. PLoS Genet. *9*, e1003855.

De Arras, L., Seng, A., Lackford, B., Keikhaee, M.R., Bowerman, B., Freedman, J.H., Schwartz, D.A., and Alper, S. (2013). An evolutionarily conserved innate immunity protein interaction network. J. Biol. Chem. *288*, 1967–1978.

Gray, P., Michelsen, K.S., Sirois, C.M., Lowe, E., Shimada, K., Crother, T.R., Chen, S., Brikos, C., Bulut, Y., Latz, E., et al. (2010). Identification of a novel human MD-2 splice variant that negatively regulates Lipopolysaccharide-induced TLR4 signaling. J. Immunol. *184*, 6359–6366.

Higa, M., Oka, M., Fujihara, Y., Masuda, K., Yoneda, Y., and Kishimoto, T. (2018). Regulation of inflammatory responses by dynamic subcellular localization of RNA-binding protein Arid5a. Proc. Natl. Acad. Sci. USA *115*, E1214–E1220.

Hovhannisyan, R.H., and Carstens, R.P. (2007). Heterogeneous ribonucleoprotein m is a splicing regulatory protein that can enhance or silence splicing of alternatively spliced exons. J. Biol. Chem. *282*, 36265–36274.

Huang, Y., Yario, T.A., and Steitz, J.A. (2004). A molecular link between SR protein dephosphorylation and mRNA export. Proc. Natl. Acad. Sci. USA *101*, 9666–9670.

Huelga, S.C., Vu, A.Q., Arnold, J.D., Liang, T.Y., Liu, P.P., Yan, B.Y., Donohue, J.P., Shiue, L., Hoon, S., Brenner, S., et al. (2012). Integrative genome-wide analysis reveals cooperative regulation of alternative splicing by hnRNP proteins. Cell Rep. *1*, 167–178.

Janssens, S., Burns, K., Vercammen, E., Tschopp, J., and Beyaert, R. (2003). MyD88S, a splice variant of MyD88, differentially modulates NF-kappaB- and AP-1-dependent gene expression. FEBS Lett. *548*, 103–107.

Kalam, H., Fontana, M.F., and Kumar, D. (2017). Alternate splicing of transcripts shape macrophage response to Mycobacterium tuberculosis infection. PLoS Pathog. *13*, e1006236.

Kandasamy, R.K., Vladimer, G.I., Snijder, B., Müller, A.C., Rebsamen, M., Bigenzahn, J.W., Moskovskich, A., Sabler, M., Stefanovic, A., Scorzoni, S., et al. (2016). A time-resolved molecular map of the macrophage response to VSV infection. NPJ Syst. Biol. Appl. *2*, 16027.

Kim, S., Kim, H., Fong, N., Erickson, B., and Bentley, D.L. (2011). Pre-mRNA splicing is a determinant of histone H3K36 methylation. Proc. Natl. Acad. Sci. USA *108*, 13564–13569.

Kosugi, S., Hasebe, M., Tomita, M., and Yanagawa, H. (2009). Systematic identification of cell cycle-dependent yeast nucleocytoplasmic shuttling proteins by prediction of composite motifs. Proc. Natl. Acad. Sci. USA *106*, 10171–10176.

Lichtenstein, M., Guo, W., and Tartakoff, A.M. (2001). Control of nuclear export of hnRNP A1. Traffic *2*, 261–267.

Liepelt, A., Mossanen, J.C., Denecke, B., Heymann, F., De Santis, R., Tacke, F., Marx, G., Ostareck, D.H., and Ostareck-Lederer, A. (2014). Translation control of TAK1 mRNA by hnRNP K modulates LPS-induced macrophage activation. RNA *20*, 899–911.

Ling, J.P., Pletnikova, O., Troncoso, J.C., and Wong, P.C. (2015). TDP-43 repression of nonconserved cryptic exons is compromised in ALS-FTD. Science *349*, 650–655.

Ling, J.P., Chhabra, R., Merran, J.D., Schaughency, P.M., Wheelan, S.J., Corden, J.L., and Wong, P.C. (2016). PTBP1 and PTBP2 Repress Nonconserved Cryptic Exons. Cell Rep. *17*, 104–113.

Llères, D., Denegri, M., Biggiogera, M., Ajuh, P., and Lamond, A.I. (2010). Direct interaction between hnRNP-M and CDC5L/PLRG1 proteins affects alternative splice site choice. EMBO Rep. *11*, 445–451.

Marko, M., Leichter, M., Patrinou-Georgoula, M., and Guialis, A. (2010). hnRNP M interacts with PSF and p54(nrb) and co-localizes within defined nuclear structures. Exp. Cell Res. *316*, 390–400.

Martins, S.B., Rino, J., Carvalho, T., Carvalho, C., Yoshida, M., Klose, J.M., de Almeida, S.F., and Carmo-Fonseca, M. (2011). Spliceosome assembly is coupled to RNA polymerase II dynamics at the 3′ end of human genes. Nat. Struct. Mol. Biol. *18*, 1115–1123.

Masuda, K., Ripley, B., Nishimura, R., Mino, T., Takeuchi, O., Shioi, G., Kiyonari, H., and Kishimoto, T. (2013). Arid5a controls IL-6 mRNA stability, which contributes to elevation of IL-6 level in vivo. Proc. Natl. Acad. Sci. USA *110*, 9409–9414.

Moehle, E.A., Ryan, C.J., Krogan, N.J., Kress, T.L., and Guthrie, C. (2012). The yeast SR-like protein Npl3 links chromatin modification to mRNA processing. PLoS Genet. *8*, e1003101.

Moehle, E.A., Braberg, H., Krogan, N.J., and Guthrie, C. (2014). Adventures in time and space: splicing efficiency and RNA polymerase II elongation rate. RNA Biol. *11*, 313–319.

Neves, L.T., Douglass, S., Spreafico, R., Venkataramanan, S., Kress, T.L., and Johnson, T.L. (2017). The histone variant H2A.Z promotes efficient cotranscriptional splicing in *S. cerevisiae*. Genes Dev. *31*, 702–717.

Nissen, K.E., Homer, C.M., Ryan, C.J., Shales, M., Krogan, N.J., Patrick, K.L., and Guthrie, C. (2017). The histone variant H2A.Z promotes splicing of weak introns. Genes Dev. *31*, 688–701.

Nojima, T., Gomes, T., Carmo-Fonseca, M., and Proudfoot, N.J. (2016). Mammalian NET-seq analysis defines nascent RNA profiles and associated RNA processing genome-wide. Nat. Protoc. *11*, 413–428.

Ostareck, D.H., and Ostareck-Lederer, A. (2019). RNA-Binding Proteins in the Control of LPS-Induced Macrophage Response. Front. Genet. *10*, 31.

Ostareck-Lederer, A., Ostareck, D.H., Cans, C., Neubauer, G., Bomsztyk, K., Superti-Furga, G., and Hentze, M.W. (2002). c-Src-mediated phosphorylation of hnRNP K drives translational activation of specifically silenced mRNAs. Mol. Cell. Biol. *22*, 4535–4543.

Pai, A.A., Baharian, G., Pagé Sabourin, A., Brinkworth, J.F., Nédélec, Y., Foley, J.W., Grenier, J.-C., Siddle, K.J., Dumaine, A., Yotova, V., et al. (2016). Widespread Shortening of 3′ Untranslated Regions and Increased Exon Inclusion Are Evolutionarily Conserved Features of Innate Immune Responses to Infection. PLoS Genet. *12*, e1006338.

Pandey, A., Ding, S.L., Qin, Q.-M., Gupta, R., Gomez, G., Lin, F., Feng, X., Fachini da Costa, L., Chaki, S.P., Katepalli, M., et al. (2017). Global Reprogramming of Host Kinase Signaling in Response to Fungal Infection. Cell Host Microbe *21*, 637–649.

Pandya-Jones, A., and Black, D.L. (2009). Co-transcriptional splicing of constitutive and alternative exons. RNA *15*, 1896–1908.

Pandya-Jones, A., Bhatt, D.M., Lin, C.-H., Tong, A.-J., Smale, S.T., and Black, D.L. (2013). Splicing kinetics and transcript release from the chromatin compartment limit the rate of Lipid A-induced gene expression. RNA *19*, 811–827.

Park, E., Iaccarino, C., Lee, J., Kwon, I., Baik, S.M., Kim, M., Seong, J.Y., Son, G.H., Borrelli, E., and Kim, K. (2011). Regulatory roles of heterogeneous nuclear ribonucleoprotein M and Nova-1 protein in alternative splicing of dopamine D2 receptor pre-mRNA. J. Biol. Chem. *286*, 25301–25308.

Passacantilli, I., Frisone, P., De Paola, E., Fidaleo, M., and Paronetto, M.P. (2017). hnRNPM guides an alternative splicing program in response to inhibition of the PI3K/AKT/mTOR pathway in Ewing sarcoma cells. Nucleic Acids Res. *45*, 12270–12284.

Patrick, K.L., Ryan, C.J., Xu, J., Lipp, J.J., Nissen, K.E., Roguev, A., Shales, M., Krogan, N.J., and Guthrie, C. (2015). Genetic interaction mapping reveals a role for the SWI/SNF nucleosome remodeler in spliceosome activation in fission yeast. PLoS Genet. *11*, e1005074.

Penn, B.H., Netter, Z., Johnson, J.R., Von Dollen, J., Jang, G.M., Johnson, T., Ohol, Y.M., Maher, C., Bell, S.L., Geiger, K., et al. (2018). An Mtb-Human Protein-Protein Interaction Map Identifies a Switch between Host Antiviral and Antibacterial Responses. Mol. Cell *71*, 637–648.

Pettit Kneller, E.L., Connor, J.H., and Lyles, D.S. (2009). hnRNPs Relocalize to the cytoplasm following infection with vesicular stomatitis virus. J. Virol. *83*, 770–780.

Poltorak, A., He, X., Smirnova, I., Liu, M.Y., Van Huffel, C., Du, X., Birdwell, D., Alejos, E., Silva, M., Galanos, C., et al. (1998). Defective LPS signaling in C3H/HeJ and C57BL/10ScCr mice: mutations in Tlr4 gene. Science *282*, 2085–2088.

Ramirez-Carrozzi, V.R., Braas, D., Bhatt, D.M., Cheng, C.S., Hong, C., Doty, K.R., Black, J.C., Hoffmann, A., Carey, M., and Smale, S.T. (2009). A unifying model for the selective regulation of inducible transcription by CpG islands and nucleosome remodeling. Cell *138*, 114–128.

Rao, N., Nguyen, S., Ngo, K., and Fung-Leung, W.-P. (2005). A novel splice variant of interleukin-1 receptor (IL-1R)-associated kinase 1 plays a negative regulatory role in Toll/IL-1R-induced inflammatory signaling. Mol. Cell. Biol. *25*, 6521–6532.

Saldi, T., Cortazar, M.A., Sheridan, R.M., and Bentley, D.L. (2016). Coupling of RNA Polymerase II Transcription Elongation with Pre-mRNA Splicing. J. Mol. Biol. *428*, 2623–2635.

Seo, J.-W., Yang, E.-J., Kim, S.H., and Choi, I.-H. (2015). An inhibitory alternative splice isoform of Toll-like receptor 3 is induced by type I interferons in human astrocyte cell lines. BMB Rep. *48*, 696–701.

Shin, C., Feng, Y., and Manley, J.L. (2004). Dephosphorylated SRp38 acts as a splicing repressor in response to heat shock. Nature *427*, 553–558.

Shin, D.-L., Hatesuer, B., Bergmann, S., Nedelko, T., and Schughart, K. (2015). Protection from Severe Influenza Virus Infections in Mice Carrying the Mx1 Influenza Virus Resistance Gene Strongly Depends on Genetic Background. J. Virol. *89*, 9998–10009.

Stamm, S. (2008). Regulation of alternative splicing by reversible protein phosphorylation. J. Biol. Chem. *283*, 1223–1227.

Stetson, D.B., and Medzhitov, R. (2006). Recognition of cytosolic DNA activates an IRF3-dependent innate immune response. Immunity *24*, 93–103.

Sun, H., Kamanova, J., Lara-Tejero, M., and Galán, J.E. (2018). Salmonella stimulates pro-inflammatory signalling through p21-activated kinases bypassing innate immune receptors. Nat. Microbiol. *3*, 1122–1130.

Thomas, P., Forse, R.A., and Bajenova, O. (2011). Carcinoembryonic antigen (CEA) and its receptor hnRNP M are mediators of metastasis and the inflammatory response in the liver. Clin. Exp. Metastasis *28*, 923–932.

Van Nostrand, E.L., Pratt, G.A., Shishkin, A.A., Gelboin-Burkhart, C., Fang, M.Y., Sundararaman, B., Blue, S.M., Nguyen, T.B., Surka, C., Elkins, K., et al. (2016). Robust transcriptome-wide discovery of RNA-binding protein binding sites with enhanced CLIP (eCLIP). Nat. Methods *13*, 508–514.

Vaquero-Garcia, J., Barrera, A., Gazzara, M.R., González-Vallinas, J., Lahens, N.F., Hogenesch, J.B., Lynch, K.W., and Barash, Y. (2016). A new view of transcriptome complexity and regulation through the lens of local splicing variations. eLife *5*, e11752.

Viktorovskaya, O.V., Greco, T.M., Cristea, I.M., and Thompson, S.R. (2016). Identification of RNA Binding Proteins Associated with Dengue Virus RNA in Infected Cells Reveals Temporally Distinct Host Factor Requirements. PLoS Negl. Trop. Dis. *10*, e0004921.

Xu, Y., Gao, X.D., Lee, J.-H., Huang, H., Tan, H., Ahn, J., Reinke, L.M., Peter, M.E., Feng, Y., Gius, D., et al. (2014). Cell type-restricted activity of hnRNPM promotes breast cancer metastasis via regulating alternative splicing. Genes Dev. *28*, 1191–1203.

Yachdav, G., Kloppmann, E., Kajan, L., Hecht, M., Goldberg, T., Hamp, T., Hönigschmid, P., Schafferhans, A., Roos, M., Bernhofer, M., et al. (2014). PredictProtein–an open resource for online prediction of protein structural and functional features. Nucleic Acids Res. *42*, W337–W343.

Yamamoto, M., Sato, S., Hemmi, H., Hoshino, K., Kaisho, T., Sanjo, H., Takeuchi, O., Sugiyama, M., Okabe, M., Takeda, K., and Akira, S. (2003). Role of adaptor TRIF in the MyD88-independent toll-like receptor signaling pathway. Science *301*, 640–643.

Zhao, W., Wang, L., Zhang, M., Wang, P., Qi, J., Zhang, L., and Gao, C. (2012). Nuclear to cytoplasmic translocation of heterogeneous nuclear ribonucleoprotein U enhances TLR-induced proinflammatory cytokine production by stabilizing mRNAs in macrophages. J. Immunol. *188*, 3179–3187.

STAR★METHODS

KEY RESOURCES TABLE

REAGENT or RESOURCE	SOURCE	IDENTIFIER
Antibodies		
Rabbit polyclonal hnRNP M	Abcam	#177957
Mouse monoclonal β-Actin	Abcam	Cat#6276; RRID:AB_2223210
Rabbit polyclonal Histone 3	Abcam	Cat#1791
Mouse monoclonal hnRNP L	Abcam	Cat#6106-100; RRID:AB_305294
Rabbit polyclonal β-Tubulin	Abcam	Cat#179513
Mouse Monoclonal ANTI-FLAG M2	Sigma-Aldrich	Cat#F3165; RRID:AB_259529
Mouse monoclonal hnRNP U	Santa-Cruz	Cat#sc-32315
Alexa Fluor-488 goat anti-rabbit	Invitrogen	Cat#A-11034
IR Dye CW800 goat anti-mouse	LI-COR	Cat#925-32210
Alexa Fluor-647 goat anti-mouse	Invitrogen	Cat#A21235
IR Dye CW 680 goat anti-rabbit	LI-COR	Cat#926-68071
Bacterial and Virus Strains		
Salmonella enterica (SL1344)	Dr. Helene Andrews-Polymenis, TAMHSC	N/A
Recombinant Vesicular stomatitis virus (VSV; Indiana serotype) containing a GFP reporter cloned downstream of the VSV G-glycoprotein (VSV-G/GFP)	Dr. John Rose, Yale School of Medicine	N/A
Chemicals, Peptides, and Recombinant Proteins		
Flag Peptide	Sigma-Aldrich	Cat#F4799
Critical Commercial Assays		
ELISA MAX Mouse Standard Set IL-6	BioLegend	Cat#431301
Viromer Blue	Lipocalyx	Cat#VB-01LB-0
Experimental Models: Cell Lines		
RAW 264.7	ATCC	N/A
3xFLAG_hnRNPM RAW264.7 macrophages	This paper	N/A
hnRNPM shRNA SCR RAW 264.7 macrophages	This paper	N/A
hnRNPM shRNA M1 KD RAW 264.7 macrophages	This paper	N/A
hnRNPM shRNA M2 KD RAW 264.7 macrophages	This paper	N/A
3xFLAG_hnRNPM S85A RAW264.7 macrophages	This paper	N/A
3xFLAG_hnRNPM S85D RAW264.7 macrophages	This paper	N/A
3xFLAG_hnRNPM S431A RAW264.7 macrophages	This paper	N/A
3xFLAG_hnRNPM S431D RAW264.7 macrophages	This paper	N/A
3xFLAG_hnRNPM S480A RAW264.7 macrophages	This paper	N/A
3xFLAG_hnRNPM S480D RAW264.7 macrophages	This paper	N/A
3xFLAG_hnRNPM S574A RAW264.7 macrophages	This paper	N/A
3xFLAG_hnRNPM S574D RAW264.7 macrophages	This paper	N/A
3xFLAG_hnRNPM S636A RAW264.7 macrophages	This paper	N/A
3xFLAG_hnRNPM S636D RAW264.7 macrophages	This paper	N/A
Oligonucleotides		
See Table S4		N/A
Recombinant DNA/RNA		
Silencer Select GAPDH Positive Control siRNA	ThermoFisher	Cat#4390849
Silencer Select Negative Control No. 1 siRNA	ThermoFisher	Cat#4390843
heterogeneous nuclear ribonucleoprotein M siRNA	ThermoFisher	Cat#4390771

(*Continued on next page*)

Continued

REAGENT or RESOURCE	SOURCE	IDENTIFIER
Software and Algorithms		
CLC Genomics Workbench 8.0.1	QIAGEN Bioinformatics	https://www.qiagenbioinformatics.com/products/clc-genomics-workbench/
Ingenuity Pathway Analysis	QIAGEN Bioinformatics	N/A
MAJIQ	Vaquero-Garcia et al., 2016	https://majiq.biociphers.org/
VOILA	Vaquero-Garcia et al., 2016	https://majiq.biociphers.org/
Other		
RNA-seq raw and filtered data from hnRNP M/SCR resting and *Salmonella* infected macrophages	This paper	GEO #GSE137603

LEAD CONTACT AND MATERIALS AVAILABILITY

Requests for resources and reagents should be directed to and will be fulfilled by the Lead Contact, Robert Watson (robert.watson@tamu.edu). All unique/stable reagents generated in this study are available from the Lead Contact with a completed Materials Transfer Agreement.

EXPERIMENTAL MODEL AND SUBJECT DETAILS

Cell lines

RAW 264.7 macrophages

RAW 264.7 macrophages (ATCC) (originally isolated from male BALB/c mice) were cultured at 37°C with a humidified atmosphere of 5% CO_2 in DMEM (Thermo Fisher) with 10% FBS (Sigma Aldrich) 0.5% HEPES (Thermo Fisher). For RAW 264.7 macrophages stably expressing scramble knockdown and hnRNP M knockdown, cells were transfected with scramble non-targeting shRNA constructs and hnRNP M shRNA constructs targeted toward the 3′ UTR of hnRNP M. After 48 hours, media was supplemented with hygromycin (Invitrogen) to select for cells containing the shRNA plasmid. RAW 264.7 macrophages stably expressing GFP-FL and hnRNP M-FL were transfected for 48 hours and then selected through addition of puromycin (Invivogen).

BMDMs

Eight-week-old male C57BL/6J mice were used to generate bone marrow derived macrophages (BMDMs). All animals were housed, bred at Texas A&M Health Science Center under approved IACUC guidelines. BMDMs were differentiated from BM cells isolated by washing mouse femurs with 10 mL DMEM. Cells were then centrifuged for 5 min at 1000 rpm and resuspended in BMDM media (DMEM, 20% FBS (Millipore), 1mM sodium pyruvate (Lonza), 10% MCSF conditioned media (Waston lab)). BM cells were counted and plated at $3x10^6$ in 15 cm non-TC treated dishes in 30 mL complete BMDM media. Cells were fed with an additional 15 mL of BMDM media on day 3 of culture. Cells were harvested on day 7 with 1 X PBS EDTA (Lonza).

Bacterial strains

Salmonella enterica serovar Typhimurium (SL1344) was obtained from Helene Andrews-Polymenis, TAMHSC. Infections with *S.* Typhimurium were conducted by plating RAW 264.7 macrophages on tissue-cultured treated 12-well dishes at $7.5 x10^5$ and incubated overnight. Overnight cultures of S. Typhimurium were diluted 1:20 in LB broth containing 0.3M NaCl and grown until they reached an OD600 of 0.9.

Viral strain

Recombinant Vesicular stomatitis virus (VSV; Indiana serotype) containing a GFP reporter cloned downstream of the VSV G-glycoprotein (VSV-G/GFP) was obtained collaboratively from Dr. John Rose at Yale School of Medicine with Dr. A. Phillip West.

METHOD DETAILS

RNA-SEQ

The RNA-Seq experiment was made up of 12 samples: biological triplicate of SCR uninfected, SCR *Salmonella*-infected, hnRNP M1 uninfected, and *Salmonella*-infected hnRNP M1. RNA-Seq and library prep was performed by Texas A&M AgriLife Genomics and Bioinformatics Service. Samples were sequenced on Illumina 4000 using 2 × 75-bp paired-end reads. Raw reads were filtered and trimmed and Fastq data was mapped to the *Mus musculus* Reference genome (RefSeq) using CLC Genomics Workbench 8.0.1. Differential expression analyses were performed using CLC Genomics Workbench. Relative transcript expression was calculated by counting Reads Per Kilobase of exon model per Million mapped reads (RPKM). The differentially expressed genes were selected as those with p value threshold < 0.05 and a fold change value > 1.5 to include in the heatmaps represented. Follow up

RT-qPCR analysis was done with both knockdowns, while the best knockdown (M1) was selected for sequencing, as the phenotype often tracked with the knockdown efficiency (M1 = ~80%, M2 = ~60%). Genes with p values < 0.05 were displayed in volcano plots and heatmaps using GraphPad Prism software (GraphPad, San Diego, CA).

S. Typhimurium Infection

Unless specified, cell lines at a confluency of 80% were infected with the S. Typhimurium strains at an MOI of 10 for 30 minutes in Hank's buffered salt solution (HBSS), and subsequently cells were spun for 10 minutes at 1,000rpm, washed twice in HBSS containing 100μg/ml of gentamycin, and refilled with media plus gentamicin (10 μg/ml). Supernatants were collected at 2 hours and 4 hours and analyzed using IL6 ELISA (Biolegend). After removal of supernatant, cells were lysed in Trizol (Thermo Fisher) for RNA collection and analyzed using RT-qPCR.

LPS Treatment

RAW 264.7 macrophages were plated on 12-well tissue-culture treated plates at a density of $7.5x10^5$ and allowed to acclimate overnight. Cells were then treated with E. Coli Lipopolysaccharide (Sigma-Aldrich) at 100ng/mL for the respective time points where supernatants and RNA were collected for analysis.

Immunofluorescence Microscopy

RAW 264.7 macrophages were plated on glass coverslips in 48-well plates. Cells were treated with LPS as described above. At the designated time points, cells were washed with PBS (Thermo Fisher) and then fixed in 4% paraformaldehyde for 10 minutes. Cells were washed with PBS 3x and then permeabilized with 0.2% Triton-X (Thermo Fisher). Coverslips were placed in primary antibody for 1 hour then washed 3x in PBS and placed in secondary antibody. These were washed twice in PBS and twice in deionized water, followed by mounting onto a glass slide using ProLong Diamond antifade mountant (Invitrogen). Images were acquired on a Nikon A1-Confocal Microscope.

Western Blots

Protein samples were run on Any kD Mini-PROTEAN TGX precast protein gels (BioRad) and transferred to 0.45 um nitrocellulose membranes (GE Healthcare). The membranes were incubated in the primary antibody of interest overnight and washed with TBS-Tween 20. Membranes were then incubated in secondary antibody for 1-2 hours and imaged using LI-COR Odyssey FC Imaging System.

siRNA Transfection

BMDMs were plated at $3x10^5$ in 12-well TC-treated plates and incubated overnight. Viromer Blue (Lipocalyx) was used to transfect siRNAs according to the manufacturer's instructions. The siRNAs directed against Gapdh and hnRNP M were purchased from Thermo Fisher with a negative control present. After 48 hr of siRNA transfection, LPS was added and RNA was collected at the respective time points.

Antibodies

The following primary antibodies were used: rabbit polyclonal hnRNP M (Abcam, #177957), rabbit polyclonal Histone 3 (Abcam, #1791), mouse monoclonal Beta-Actin (Abcam, #6276), mouse monoclonal hnRNP L (Abcam, #6106-100), rabbit polyclonal Beta-Tubulin (Abcam, #179513), mouse monoclonal hnRNP U (Santa-Cruz, sc-32315), DAPI nuclear staining (Thermo Fisher), and mouse monoclonal ANTI-FLAG M2 antibody (Sigma-Aldrich, F3165). Secondary antibodies used were as follows: IR Dye CW 680 goat anti-rabbit, IR Dye CW800 goat anti-mouse (LI-COR), Alexfluor-488 anti-rabbit and Alexafluo-647 anti-mouse secondary antibodies for immunofluorescence (LI-COR).

Cellular fractionation

Macrophage cellular fractionation was done as described in Pandya-Jones et al., 2013. Briefly, RAW 264.7 macrophages were plated on in 10 cm tissue-culture treated plates at $1\text{-}3x10^7$ per plate. Cells and buffers were kept on ice unless noted otherwise. Cells were rinsed twice in cold PBS-EDTA (Lonza) and scraped into 15 mL conical tubes. Cells were spun at 1,000 g for 5 minutes at 4C and resuspended in NP-40 lysis buffer (10 mM Tris-HCl [pH 7.5], 0.05% NP40 [Sigma], 150 mM NaCl, protease inhibitor tablet (Thermo Fisher)) and incubated for 5 min on ice. Lysate was added to 2.5 volumes of a sucrose cushion (Lysis buffer with 24% sucrose) and centrifuged for at 14,000 rpm for 10min at 4C. The supernatant was collected and saved for cytoplasmic protein sample. The nuclear pellet was resuspended in glycerol buffer (20 mM Tris-HCl [pH 7.9], 75 mM NaCl, 0.5 mM EDTA, 0.85 mM DTT, 50% glycerol, protease inhibitor tablet) and lysed with nuclear lysate buffer in equal volume and vortexed 2X for 2 s (10 mM HEPES [pH 7.6], 1 mM DTT, 7.5 mM $MgCl_2$, 0.2 mM EDTA, 0.3 M NaCl, 1 M UREA, 1% NP-40, protease inhibitor tablet). Lysates were chilled on ice for 2 minutes and then spun at 10,000 rpm for 2 minutes at 4C. Supernatant was collected and used for nucleoplasmic protein samples. The remining chromatin pellet was gently rinsed in PBS-EDTA and treated with DNase in DNase buffer for 1 hr at 37C. After incubation, the

supernatant was collected for chromatin protein samples. Sample buffer (BIO-RAD) and 2-Mercapoethanol (BIO-RAD) was added to every protein sample with 5 minutes boiling prior to running on gels for western blots. Approximately 10% of sample was loaded for western blots.

RNase Fractionation

For nuclear lysates treated with RNase, nuclear pellets were responded in glycerol buffer. Nuclear lysis buffer was added, and lysates were incubated on ice for 5 minutes. Samples were then divided into two samples with one receiving 1 ul of RNase A (Thermo Fisher) per 50 ul sample and another with no RNase A. Both were incubated at 37C for 30 mins. Lysates were then spun at 10,000rpm for 2 mins and the rest of the fractionation proceeded as described.

Gene Ontology (GO) Canonical Pathway Analysis

To determine the most affected pathways in control versus hnRNP M knockdown RAW 264.7 macrophages, canonical pathway analysis was conducted using Ingenuity Pathway Analysis software from QIAGEN Bioinformatics. Genes that were differentially expressed wth a p value < 0.05 from our RNA-SEQ analysis were used as input from uninfected and *Salmonella* Typhimurium infected cells. The top hits were represented in bar graphs by z-score.

RNA isolation and qPCR analysis

For transcript analysis, cells were harvested in Trizol and RNA was isolated using Direct-zol RNA Miniprep kits (Zymo Research) with 1 hr DNase treatment. cDNA was synthesized with iScript cDNA Synthesis Kit (Bio-Rad). CDNA was diluted to 1:20 for each sample. A pool of cDNA from each treated or infected sample was used to make a 1:10 standard curve with each standard sample diluted 1:5 to produce a linear curve. RT-qPCR was performed using Power-Up SYBR Green Master Mix (Thermo Fisher) using a Quant Studio Flex 6 (Applied Biosystems). Samples were run in triplicate wells in a 96-well plate. Averages of the raw values were normalized to average values for the same sample with the control gene, beta-actin. To analyze fold induction, the average of the treated sample was divided by the untreated control sample, which was set at 1.

Chromatin Immunoprecipitation

Chromatin Immunoprecipitation (ChIP) was adapted from Abcam's protocol. Briefly, two confluent 15 cm dishes of RAW 264.7 macrophages were crosslinked in formaldehyde to a final concentration of 0.75% and rotated for 10 minutes. Glycine was added to stop the cross linking by shaking for 5 minutes at a concentration of 125 mM. Cells were rinsed with PBS twice and then scraped into 5 mL PBS and centrifuged at 1,000 g for 5 min at 4C. Cellular pellets were resuspended in ChIP lysis buffer (750 μL per $1x10^7$ cells) and incubated for 10 min on ice. Cellular lysates were sonicated for 40 minutes (30sec ON, 30sec OFF) on high in a Bioruptor UCD-200 (Diagenode). After sonication, cellular debris was pelleted by centrifugation for 10 min, 4°C, 8,000 x g. Input samples were taken at this step and stored at −80C until decrosslinking. For RNase treated samples, RNase A was added to cell lysates and incubated for 30 mins at 37C. Approximately 25 μg of DNA diluted to 1:10 with RIPA buffer was used for overnight immunoprecipitation. Each ChIP had one sample for the specific antibody and one sample for Protein G beads only which were pre-blocked for 1 hr with single stranded herring sperm DNA (75 ng/μL) and BSA (0.1 μg/μL). The respective primary antibody was added to all samples except the beads-only sample at a concentration of 5 ug and rotated at 4°C overnight. Beads were washed 3x in with a final wash in high salt (500mM NaCl). DNA was eluted with elution buffer and rotated for 15 min at 30C. Centrifuge for 1 min at 2,000 x g and transfer the supernatant into a fresh tube. Supernatant was incubated in NaCl, RNase A (10 mg/mL) and proteinase K (20 mg/mL) and incubated at 65°C for 1 h. The DNA was purified using phenol:chloroform extraction. DNA levels were measure by RT-qPCR. Primers were designed by tiling each respective gene every 500 base pairs that were inputted into NCBI primer design.

FLAG Chromatin Immunoprecipitation

In RAW 264.7 macrophages stably expressing FL-hnRNP M or FL-GFP, ChIP was conducted as described above with minor adjustments. Lysates were incubated overnight at 4C with ANTI-FLAG M2 antibody. After washing, DNA was eluted with FLAG peptide (Sigma-Aldrich F4799) by adding 20 ul of 5X FLAG peptide, vortexed at room temperature for 15 mins and supernatants were collected. This process was repeated a total of 3x followed by decrosslinking as described.

Alternative Splicing Analysis

Alternative splicing events were analyzed using MAJIQ and VOILA with the default parameters (Vaquero-Garcia et al., 2016). Briefly, uniquely mapped, junction-spanning reads were used by MAJIQ to construct splice graphs for transcripts by using the RefSeq annotation supplemented with de-novo detected junctions. Here, de-novo refers to junctions that were not in the RefSeq transcriptome database but had sufficient evidence in the RNA-Seq data. The resulting gene splice graphs were analyzed for all identified local splice variations (LSVs). For every junction in each LSV, MAJIQ then quantified expected percent spliced in (PSI) value in control and hnRNP M knockdown samples and expected change in PSI (dPSI) between control and hnRNP M KD samples. Results from VOILA were then filtered for high confidence changing LSVs (whereby one or more junctions had at least a 95% probability of expected dPSI of at least an absolute value of 20 PSI units (noted as "20% dPSI") between control and hnRNP M KD) and candidate

changing LSVs (95% probability, 10% dPSI). For the high confidence results (dPSI > = 20%), the events were further categorized as single exon cassette, multi-exon cassette, alternative 5′ and/or 3′ splice site, or intron-retention.

VSV infection

$7x10^5$ RAW cells were seeded in 12-well plates 16h before infection. Cells were infected with VSV-GFP virus(Dalton and Rose, 2001) at multiplicity of infection (MOI) of 1 and 0.1 in serum-free DMEM (HyClone SH30022.01). After 1h of incubation with media containing virus, supernatant was removed, and fresh DMEM plus 10% FBS was added to each well. At indicated times post infection, cells were harvested with Trizol and prepared for RNA isolation.

QUANTITATION AND STATISTICAL ANALYSIS

Statistical analysis of data was performed using GraphPad Prism software. Two-tailed unpaired Student's t tests were used for statistical analyses, and unless otherwise noted, all results are representative of at least three biological experiments (mean ± SEM (n = 3 per group)).

DATA AND CODE AVAILABILITY

This article contains all datasets generated during this study. All coding for Majiq and Voila was standard and is available for academic download. Raw read files for RNA-seq can be found on GEO (Accession #GSE137603).

Cell Reports, Volume *29*

Supplemental Information

The Splicing Factor hnRNP M Is a Critical Regulator of Innate Immune Gene Expression in Macrophages

Kelsi O. West, Haley M. Scott, Sylvia Torres-Odio, A. Phillip West, Kristin L. Patrick, and Robert O. Watson

Supplemental Information
West et al. 2019

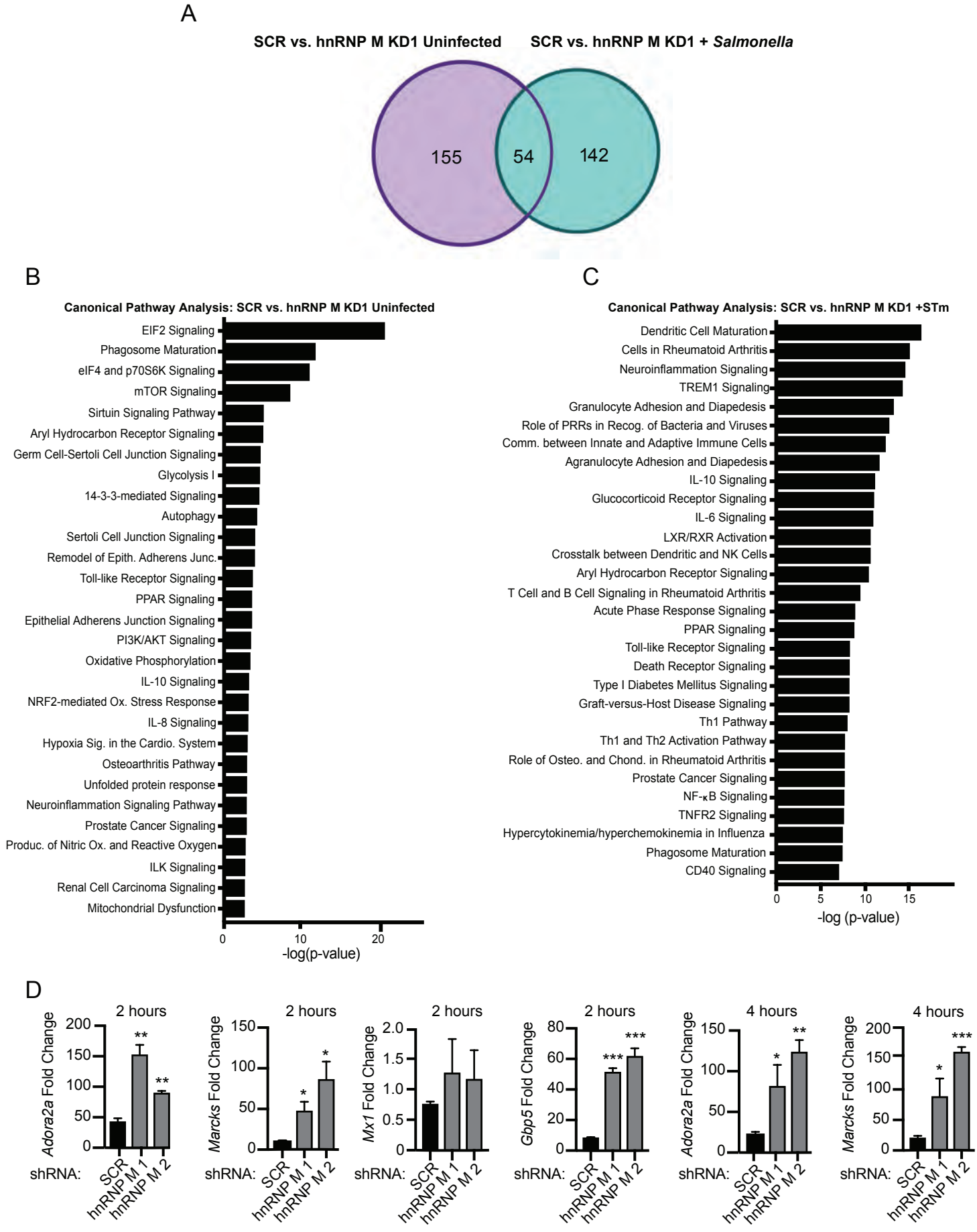

Supplemental Figure S1

Figure S1. Related to Figure 1. HnRNP M regulates expression of specific immune genes during *Salmonella* Typhimurium Infection.

(a) Venn diagram to represent overlap between hnRNP M-regulated transcripts in uninfected and *Salmonella*-infected macrophages. (b) Complete ingenuity pathway analysis for SCR vs. hnRNP M KD uninfected macrophages. (c) Complete ingenuity pathway analysis for SCR vs. hnRNP M KD *Salmonella*-infected macrophages. (d) Gene expression by RT-qPCR in SCR, hnRNP M KD 1, and hnRNP M KD 2 2hr post-*Salmonella* infection for *Adora2a, Marcks, Mx1, Gbp5,* and 4hr for *Adora2a* and *Marcks*.

RNA-Seq Uninfected		RNA-Seq +*Salmonella*	
GENE NAME	FOLD INDUCTION	GENE NAME	FOLD INDUCTION
Hpgd	13.90711	Fabp7	6.765286
Cxcr4	9.354822	Ms4a6c	5.454133
Ms4a6c	7.745006	Ms4a4c	4.956656
Csf3r	7.714053	Ms4a6d	4.288573
Fabp7	5.976491	Il6	3.957798
S1pr1	5.387236	Marcks	3.499546
Cd33	4.585221	Gm16685	3.373171
Ms4a6d	4.420621	Adora2a	3.23969
Neurl3	3.949566	Ighm	3.19321
Pros1	3.932567	Slc28a2	3.177709
Prss46	3.472838	Cfb	3.166876
Prss50	3.46898	Slamf9	3.116945
St6gal1	3.419711	Rpl27-ps3	3.017322
Ighm	3.19321	Mx1	3.008578
Cd36	3.104169	Cd36	2.828894
Il10ra	3.085386	Ctsc	2.787805
Gm12166	2.956821	C3	2.569081
Fabp4	2.923715	Fcgr3	2.480588
Aph1c	2.916988	Fabp3	2.4082
Fosb	2.85088	Smpdl3a	2.352208
Atf3	2.832853	Pld4	2.271779
Tnfrsf1b	2.814419	Nectin2	2.247367
Tgfbr1	2.740644	Dusp1	2.241607
Fcgr3	2.73009	Cd300e	2.21221
Clec4a3	2.694922	Gm5431	2.182886
Il7r	2.691738	Havcr2	2.170636
Tmem86a	2.672264	Fcgr2b	2.150546
Cav2	2.651061	Spen	2.146736
Gm6377	2.615475	C3ar1	2.115022
Cd300c2	2.58364	Cd300c2	2.104473
Fabp3	2.555074	Siglece	2.089605
Smpdl3a	2.51753	Edn1	2.089051
Ptafr	2.485913	Cd276	2.056106
Pld4	2.390038	Tgm2	2.027966
Plk2	2.379248	Fcgr4	1.997097
Btg2	2.363222	Gm10260	1.99323
C3ar1	2.210747	Il10ra	1.978782
Wfdc17	2.139324	Sema4a	1.955406
Cd276	2.135795	Ccrl2	1.938053
Itgam_1	2.060784	Ass1	1.925226
Ctsc	2.051702	Adgre1	1.866584
Egr2	2.046845	Il4i1	1.857245
Tgm2	2.039586	Pik3r6	1.817064
Egr1	1.995767	Bcl3	1.802364
Dusp1	1.995471	Tnfsf9	1.799192
Mpeg1	1.96516	Fcgr1	1.797059
Bhlhe41	1.959191	Igsf6	1.796179
Xdh	1.939404	Lacc1	1.793885
Lst1	1.919394	Zc3h12c	1.793278
Lsp1	1.897235	Gngt2	1.786466

Gnpda1	1.891593	Gm4070	1.762879
Tlr13	1.876798	Plk2	1.735775
Myo1f	1.868713	Bcl2a1a	1.731698
Rap2b	1.824333	Rsad2	1.728779
Jun	1.818452	Lsp1	1.728275
Arl11	1.803489	Cmpk2	1.716878
Rnf26_1	1.800696	Fabp4	1.709066
Havcr2	1.800502	Stat5a	1.705524
Fblim1	1.779344	Napsa	1.704077
Mcoln2	1.774978	Ppp1r15a	1.686405
Rnf128	1.761964	Gk	1.68233
Rab32	1.75113	Myo1f	1.677152
Tnfaip2	1.726583	Gpnmb	1.675334
Dhrs3	1.725571	Arhgef3	1.672991
Litaf	1.714146	Tnfaip3	1.661885
Ctsf	1.705514	Nfkbiz	1.658248
Cxcl16	1.703797	Syk	1.651344
Gstm1	1.702554	Tagap	1.645342
Gngt2	1.701373	Itgal	1.638434
Zfp385a	1.688385	Tmem51	1.636726
Pbxip1	1.687734	Mpeg1	1.635068
Hist1h1c	1.68698	Cebpb	1.63348
Gpnmb	1.672091	Dusp2	1.627537
Napsa	1.658448	Ctsf	1.621343
Fos	1.652633	Fam129a	1.620868
Cotl1	1.646704	Zfp36	1.62075
Slc15a4	1.638645	Saa3	1.617704
Tmem51	1.636726	Slc44a1	1.610821
Id3	1.631679	Ldlr	1.600648
Slc44a1	1.628823	Ptafr	1.600574
Ier2	1.613946	Fam177a	1.598248
Msrb1	1.611736	Birc3	1.591189
Il10rb	1.603	Anpep	1.587615
Bcl2a1d	1.597259	Myo1g	1.58755
Ctnnb1	1.585479	Tnfrsf1b	1.587515
Slc6a8	1.582178	Il18	1.582494
Nceh1	1.57352	Tnfaip2	1.546983
Sptssa	1.571322	Cxcl16	1.538268
Gyg	1.565705	Traf1	1.533961
Rgs2	1.565309	Gbp5	1.531947
Plin2	1.563214	Blnk	1.531359
B4galt1	1.550249	Atf3	1.530953
Rnh1	1.536697	Gadd45b	1.526009
Tbc1d16	1.521571	Lrrc25	1.515623
Zfp36	1.515133	Jak2	1.509944
Fabp5	1.507761	Icam1	1.501014
Cybb	1.506247	Capg	-1.43733
Anpep	1.50344	Ubald2	-1.50115
Alox5ap	1.500911	Rab31	-1.50144
Pdia3	-1.50295	Pdia3	-1.51841
Tubb6	-1.50417	Atp1b3	-1.5477
Tmsb10	-1.50845	Snx9	-1.56831
Sumo2	-1.53189	Ets2	-1.60419
Ccl3	-1.54719	Plau	-1.60747

Pip5k1b	-1.56974	Naa25	-1.60934
Hmga2	-1.58317	Gm26619	-1.6641
Atp1b3	-1.58414	Mrps6	-1.67118
Ank	-1.5913	Spp1	-1.67374
Cpne8	-1.59717	Tfdp1	-1.67919
Fcrl1	-1.61248	Serinc2	-1.69061
Rbpj	-1.61302	Tmem98	-1.70829
Tfdp1	-1.61335	Dhrs9	-1.71239
Slc6a12	-1.61529	Rpl10-ps3	-1.73337
Snx9	-1.62045	Spink5	-1.77682
Prelid2	-1.64498	Epn2	-1.79498
Slc16a3	-1.65921	Ccz1	-1.81366
Fosl2	-1.65925	Ier3	-1.86244
Mrps6	-1.68031	Acy1	-1.8627
Acot7	-1.71671	Ccl17	-1.86471
Oas2	-1.71742	Ccnd1	-1.87697
Ehd1	-1.75186	Lif	-1.88307
Ccnd1	-1.78697	Rgs16	-1.91798
Marcksl1	-1.81918	Csf3	-1.99019
Bnip3	-1.84262	Npl	-2.01377
Ak4	-1.84773	Timp1	-2.02017
Ets2	-1.85673	Hmga2	-2.04688
Acy1	-1.86399	Ccl2	-2.14895
Isg15	-1.88973	Dmpk	-2.16457
Odc1	-1.95677	Tnfsf15	-2.17432
Gm28037	-1.96705	Odc1	-2.24711
Layn	-1.96945	Pdia3	-2.34015
Naa25	-2.00186	Scin	-2.42501
Plekha3	-2.06644	Car2	-2.49682
Ccz1	-2.12175	Kbtbd11	-2.58657
Gm9803	-2.13322	Ccl7	-2.59416
Rtp4	-2.18593	Hnrnpm	-2.72047
Npl	-2.19264	Gm18445	-2.80579
Spp1	-2.25665	Slc6a4	-2.88423
Dmpk	-2.4654	Dmwd	-3.67138
Emp2	-2.65804	Mmp9	-3.86347
Hnrnpm	-2.69036	Tnfsf8	-4.12014
Fosl1	-2.78138	Sema7a	-4.72083
Spink5	-2.80455		
Gm18445	-2.80579		
Tmem26	-3.02585		
Flt1	-3.09266		
Serinc2	-3.27645		
Rgs16	-3.53479		
Car2	-3.73217		
Gm21987	-4.1013		
Dmwd	-4.16092		
Slc6a4	-4.72442		
Mmp9	-6.9746		
1810011H11Rik	2.333564		
AB124611	1.783388		

Table S1

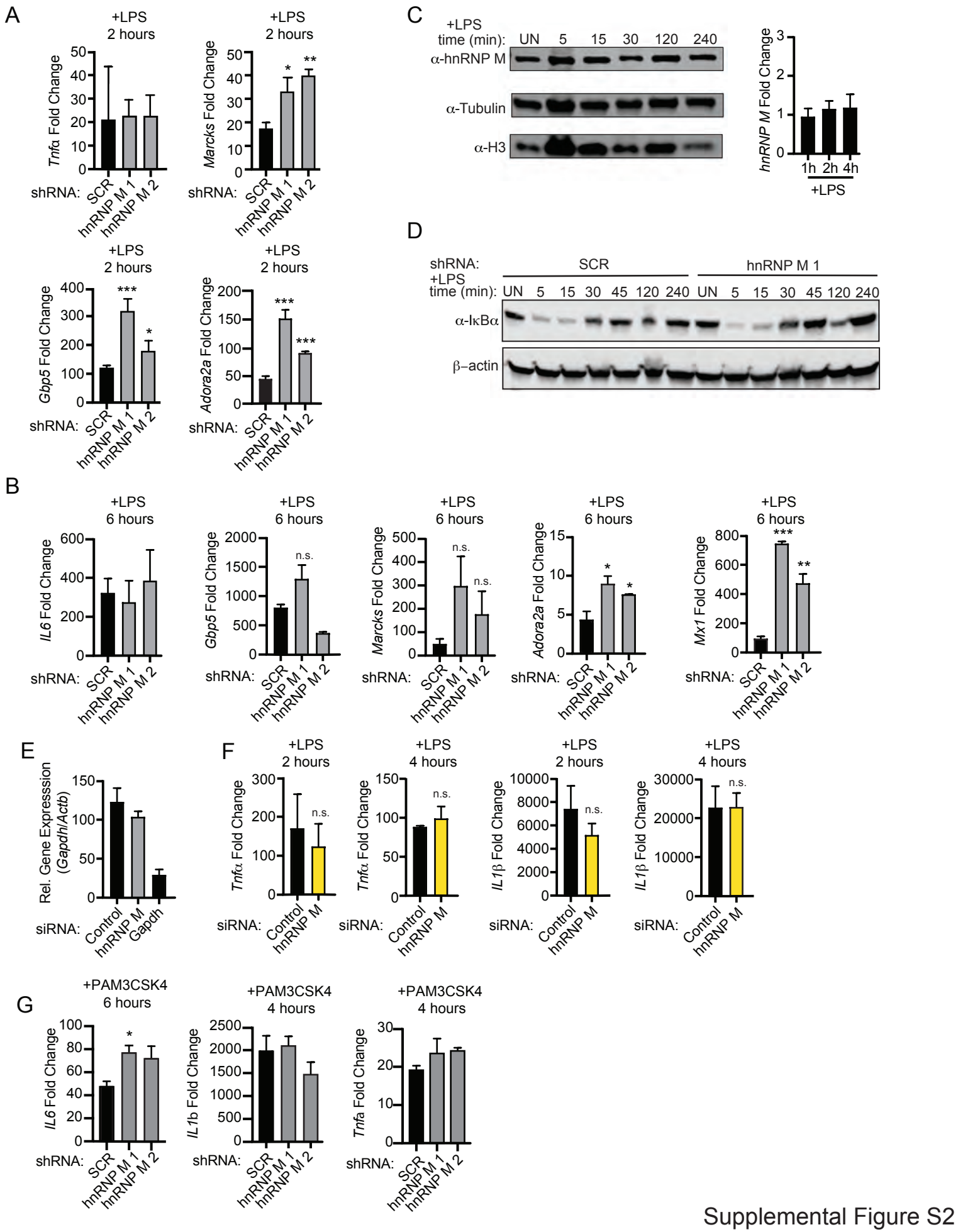

Supplemental Figure S2

Figure S2. Related to Figure 2. hnRNP M-dependent gene expression profiles are similar amongst diverse immune stimuli.

(a) *Tnfα, Marcks, Gbp5,* and *Adora2a* expression by RT-qPCR in LPS-treated cells of SCR, hnRNP M KD 1, and hnRNP M KD 2 2hr post-treatment. (b) *IL6, Gbp5, Marcks, Adora2a,* and *Mx1* expression by RT-qPCR in SCR, hnRNP M KD1, and hnRNP M KD 2 6hr post-LPS treatment. (c) Western blot analysis of endogenous hnRNP M in RAW 264.7 macrophages treated with LPS for 5, 15, 30, 120, and 240 mins. RT-qPCR of *hnRNP M* expression in RAW 264.7 cells treated with LPS for 1hr, 2hr, and 4hr. (d) Western blot analysis of αIKβ in SCR control and hnRNP M KD 1 macrophages treated with LPS for 5, 15, 30, 45, 120, and 240 mins. (e) RT-qPCR demonstrating effective depletion of GAPDH in siRNA transfected BMDMs. (f) RT-qPCR of *Tnfα* and *IL1ß* in negative control and hnRNP M siRNA BMDMs treated with 10 ng/ml of LPS for 2hrs and 4hrs. (g) RT-qPCR of *IL6, Tnfα,* and *IL1ß* in SCR control and hnRNP M KD macrophages treated with PAM3CSK4 for 6hrs and 4hrs.

+ *Salmonella*

Upregulated genes			Downregulated genes		
	GUGGUGG	GGUUGGUU		GUGGUGG	GGUUGGUU
Fabp7			Ubald2	+	
Ms4a6c	+		Rab31	+	+
Ms4a4c	+	+	Pdia3	+	+
Ms4a6d	+		Atp1b3	+	+
Il6	+		Snx9	+	+
Marcks	+		Ets2	+	
Gm16685	+		Plau	+	
Adora2a	+		Naa25	+	+
Slc28a2	+		Gm26619	+	
Cfb			Mrps6	+	
Slamf9			Spp1	+	
Mx1	+		Tfdp1	+	+
Cd36	+	+	Serinc2	+	
Ctsc	+		Tmem98	+	
C3	+	+	Dhrs9		
Fcgr3	+	+	Rpl10-ps3		
Fabp3			Spink5	+	
Smpd13a	+		Epn2	+	+
Pld4	+		Ccz1	+	
Nectin2	+	+	Ier3		
Dusp1			Acy1	+	
Cd300e	+		Ccl17		
Gm5431	+	+	Ccnd1	+	
Siglece	+		Lif	+	
Havcr2	+	+	Rgs16	+	
Fcgr2	+		Csf3		
Spen	+	+	Npl	+	+
C3ar1	+		Timp1	+	
Cd300c2	+		Hmga2	+	+
Edn1			Ccl2		
Cd276			Dmpk	+	
Tgm2	+	+	Tnfsf15	+	
Fcgr4	+	+	Odc1	+	
Gm10260			Gm9260		
IL10ra	+		Scin	+	+
Sema4a	+		Car2		
Ccr12			Kbtbd11	+	
Ass1	+		Ccl7		
Adgre	+	+	Hnrnpm	+	
Pik3r6	+		Slc6a4	+	+
Il4i1	+		Dmwd		
Bcl3	+		Mmp9	+	
Tnfsf9			Tnfsf8	+	
Fcgr1	+		Sema7a	+	
Igsf6	+	+			
Lacc1	+	+			
Zc3h12c	+				
Gngt2					
Plk2					
Gm4070	+				
Bcl2a1a					
Rsad2	+				
Lsp1	+	+			
Cmpk2	+				
Fabp4	+				
Stat5a	+	+			
Napsa	+				
Ppr1r15a					
Gk	+	+			
Myo1f	+				
Gpnmb	+	+			

Arhgef3	+	+			
Tnfaip3	+				
Nfkbiz	+	+			
Syk	+	+			
Tagap		+			
Itgal	+	+			
Mpeg1					
Cebpb					
Dusp2					
Ctsf					
Fam129a	+				
Zfp36					
Saa3	+				
Slc44a1	+	+			
Ldlr	+				
Ptafr	+	+			
Acp2	+				
Fam177a	+				
Birc3	+				
Anpep	+				
Myo1g	+				
Tnfrsf1b	+	+			
Il18	+				
Tnfaip2					
Cxcl16					
Traf1	+	+			
Gbp5	+				
Blnk	+				
Atf3					
Lrrc25	+				
Jak2	+	+			
Gadd45b					
Icam1	+	+			

Table S2

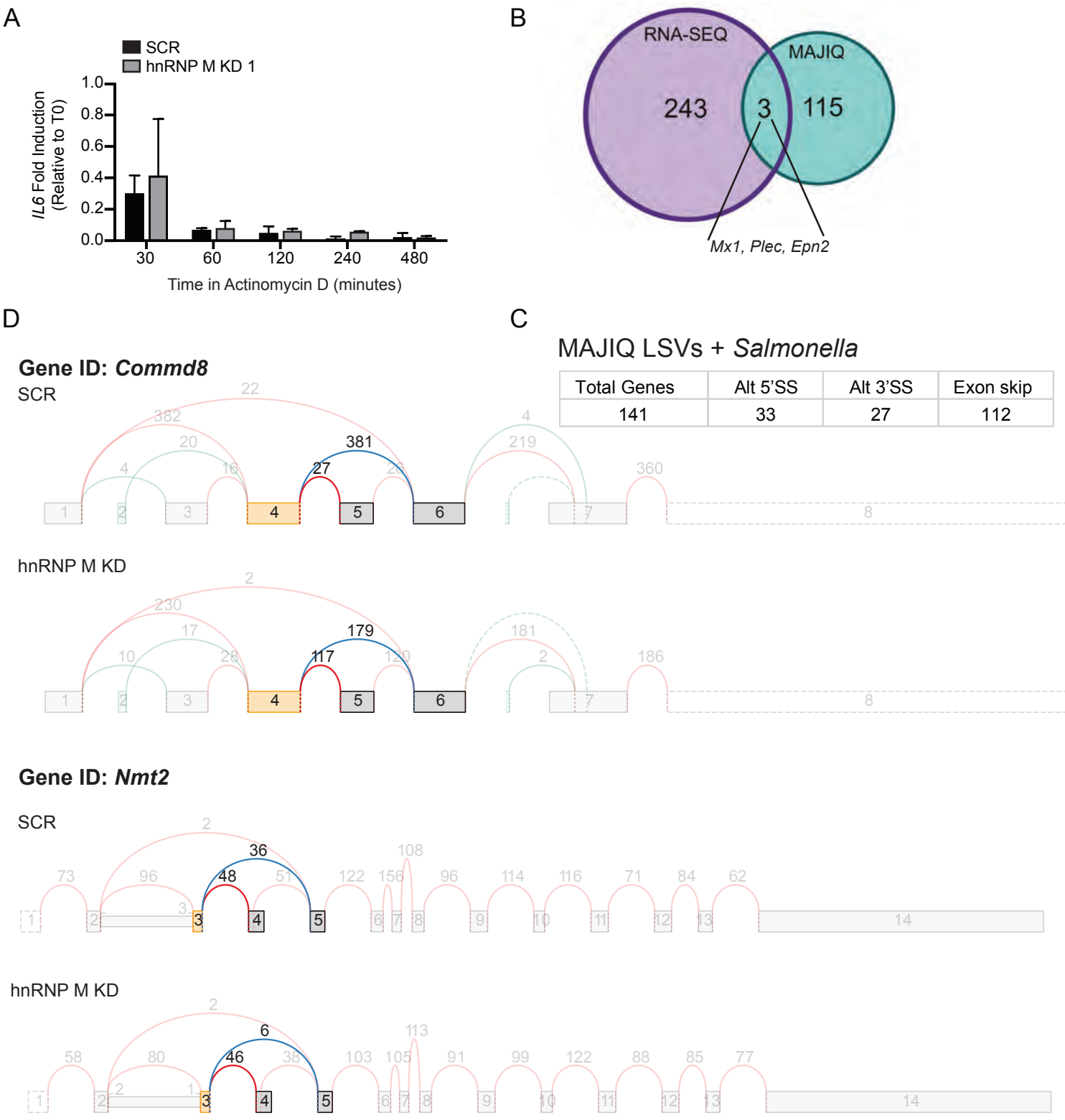

Figure S3. Related to Figure 3. hnRNP M influences gene expression outcomes at the level of pre-mRNA splicing.
(a) IL6 expression by RT-qPCR in SCR, hnRNP M KD1 cells treated with LPS for 1hr then treated with Actinomycin D for 0, 30, 60, 120, 240, and 480 mins. (b) Venn diagram to represent overlap between hnRNP M-regulated transcripts identified via RNA-Seq analysis (unique genes identified in Salmonella and uninfected analyses) and hnRNP M-dependent LSVs identified via MAJIQ analysis (total number of unique LSV events from both Salmonella and uninfected conditions). (c) Categorization of alternative splicing events identified via MAJIQ in uninfected vs. Salmonella-infected samples. (d) Full VOILA-generated tracks for Commd8 and Nmt2. Significant LSVs are shown in color.

MAJIQ GENES (UN+SAL)	Found in eCLIP (ENCODE)	RNA-Seq Uninfected	Found in eCLIP (ENCODE)	RNA-Seq +*Salmonella*	Found in eCLIP (ENCODE)
1190007I07Rik				Fabp7	
Acvr1	*	Hpgd		Ms4a6	
Aldh3a2		Cxcr4		Ms4a4c	
Amotl1	*	Ms4a6c		Ms4a6d	
Asxl1	*	Csf3r		Il6	
Atxn2	*	Fabp7		Marcks	*
Auh	*	S1pr1		Gm16685	
Ccne2		Cd33		Adora2a	*
Chka	*	Ms4a6d		Ighm	*
Cnot4	*	Neurl3		Slc28a2	
Commd8		Pros1	*	Cfb	
Dcaf8	*	Prss46		Slamf9	
Desi2	*	Prss50		Rpl27-ps3	
Dock10		St6gal1	*	Mx1	
Dtx2	*	Ighm		Cd36	
Ercc8		Cd36		Ctsc	*
Frmd4a	*	Il10ra		C3	
Gfod1	*	Gm12166		Fcgr3	
Gm29247		Fabp4		Fabp3	
Hps5		Aph1c		Smpdl3a	
Ist1	*	Fosb		Pld4	
Kat6a	*	Atf3		Nectin2	
Kat6a		Tnfrsf1b		Dusp1	
Klf7	*	Tgfbr1	*	Cd300e	
Ktn1	*	Fcgr3		Gm5431	
Lrmp		Clec4a3		Havcr2	
Mdm4	*	Il7r		Fcgr2b	
Mx1		Tmem86a		Spen	*
Nmt2	*	Cav2		C3ar1	
Numb		Gm6377		Cd300c2	
Pak1	*	Cd300c2		Siglece	
Pds5b	*	Fabp3		Edn1	
Phactr4	*	Smpdl3a	*	Cd276	*
Plec	*	Ptafr		Tgm2	
Plxnc1		Pld4		Fcgr4	
Rpl22	*	Plk2		Gm10260	
Sec14l1	*	Btg2		Il10ra	
Senp1		C3ar1		Sema4a	
Senp6	*	Wfdc17		Ccrl2	
Smc6		Cd276	*	Ass1	*
Tbc1d7		Itgam_1		Adgre1	
Tex30		Ctsc	*	Il4i1	*
Tmem87a	*	Egr2		Pik3r6	
Trmu	*	Tgm2		Bcl3	
Ubqln1	*	Egr1	*	Tnfsf9	
Xpo6		Dusp1		Fcgr1	
Zfyve27	*	Mpeg1		Igsf6	
Zmynd8	*	Bhlhe41		Lacc1	
1110051M20Rik		Xdh		Zc3h12c	
4833420G17Rik		Lst1		Gngt2	
Ankra2		Lsp1		Gm4070	
Aplp2	*	Gnpda1		Plk2	
Atf2	*	Tlr13		Bcl2a1a	
Ccdc77		Myo1f		Rsad2	
Ccdc82	*	Rap2b		Lsp1	
Clk4	*	Jun		Cmpk2	
Csnk1d	*	Arl11		Fabp4	
Def8	*	Rnf26_1		Stat5a	*
Dmac2		Havcr2		Napsa	
Ehmt1	*	Fblim1		Ppp1r15a	

Emsy	*	Mcoln2	*	Gk	
Epn2	*	Rnf128		Myo1f	
Fbxo34	*	Rab32		Gpnmb	
Foxd2os		Tnfaip2	*	Arhgef3	*
Foxo3	*	Dhrs3	*	Tnfaip3	*
Gabpb2		Litaf	*	Nfkbiz	*
Ggta1		Ctsf		Syk	
Gm46430		Cxcl16		Tagap	
Golgb1	*	Gstm1		Itgal	
Herc2	*	Gngt2		Tmem51	*
Lair1		Zfp385a		Mpeg1	
Luzp1	*	Pbxip1		Cebpb	
Lyar		Hist1h1c		Dusp2	
Mettl2		Gpnmb		Ctsf	
Mycbp2	*	Napsa		Fam129a	
Myo18a	*	Fos		Zfp36	
Ncapg2	*	Cotl1		Saa3	
Nsmaf	*	Slc15a4	*	Slc44a1	*
Panx1		Tmem51		Ldlr	
Patz1	*	Id3		Ptafr	
Ppcdc		Slc44a1	*	Fam177a	
Ppp2r5c	*	Ier2	*	Birc3	
Pradc1		Msrb1		Anpep	
Prepl		Il10rb		Myo1g	
Prr14	*	Bcl2a1d		Tnfrsf1b	
Ptger4		Ctnnb1	*	Il18	
Ptpn4	*	Slc6a8		Tnfaip2	*
Rnf20		Nceh1		Cxcl16	
Snx12		Sptssa	*	Traf1	
Sptan1		Gyg		Gbp5	
Srrm2	*	Rgs2		Blnk	
St7	*	Plin2		Atf3	
Tmem161b	*	B4galt1	*	Gadd45b	
Tmem229b		Rnh1		Lrrc25	
Tmem80		Tbc1d16		Jak2	*
Ttc13	*	Zfp36		Icam1	
Vegfa		Fabp5		Capg	*
Zmym3		Cybb		Ubald2	
		Anpep		Rab31	*
		Alox5ap		Pdia3	
		Pdia3		Atp1b3	*
		Tubb6		Snx9	*
		Tmsb10		Ets2	*
		Sumo2		Plau	*
		Ccl3		Naa25	
		Pip5k1b	*	Gm26619	
		Hmga2	*	Mrps6	*
		Atp1b3	*	Spp1	
		Ank	*	Tfdp1	*
		Cpne8	*	Serinc2	
		Fcrl1		Tmem98	
		Rbpj	*	Dhrs9	
		Tfdp1	*	Rpl10-ps3	*
		Slc6a12		Spink5	
		Snx9	*	Epn2	*
		Prelid2	*	Ccz1	
		Slc16a3		Ier3	
		Fosl2		Acy1	
		Mrps6	*	Ccl17	
		Acot7		Ccnd1	
		Oas2		Lif	
		Ehd1		Rgs16	
		Ccnd1		Csf3	
		Marcksl1	*	Npl	
		Bnip3	*	Timp1	

		Ak4	*	Hmga2	*
		Ets2	*	Ccl2	
		Acy1		Dmpk	
		Isg15		Tnfsf15	
		Odc1	*	Odc1	*
		Gm28037		Pdia3	
		Layn		Scin	
		Naa25	*	Car2	
		Plekha3		Kbtbd11	*
		Ccz1		Ccl7	
		Gm9803		Hnrnpm	*
		Rtp4		Gm18445	
		Npl		Slc6a4	
		Spp1		Dmwd	
		Dmpk		Mmp9	
		Emp2		Tnfsf8	
		Hnrnpm		Sema7a	*
		Fosl1			
		Spink5			
		Gm18445			
		Tmem26			
		Flt1			
		Serinc2			
		Rgs16			
		Car2			
		Gm21987			
		Dmwd			
		Slc6a4			
		Mmp9			
		1810011H11Rik			
		AB124611			

Table S3

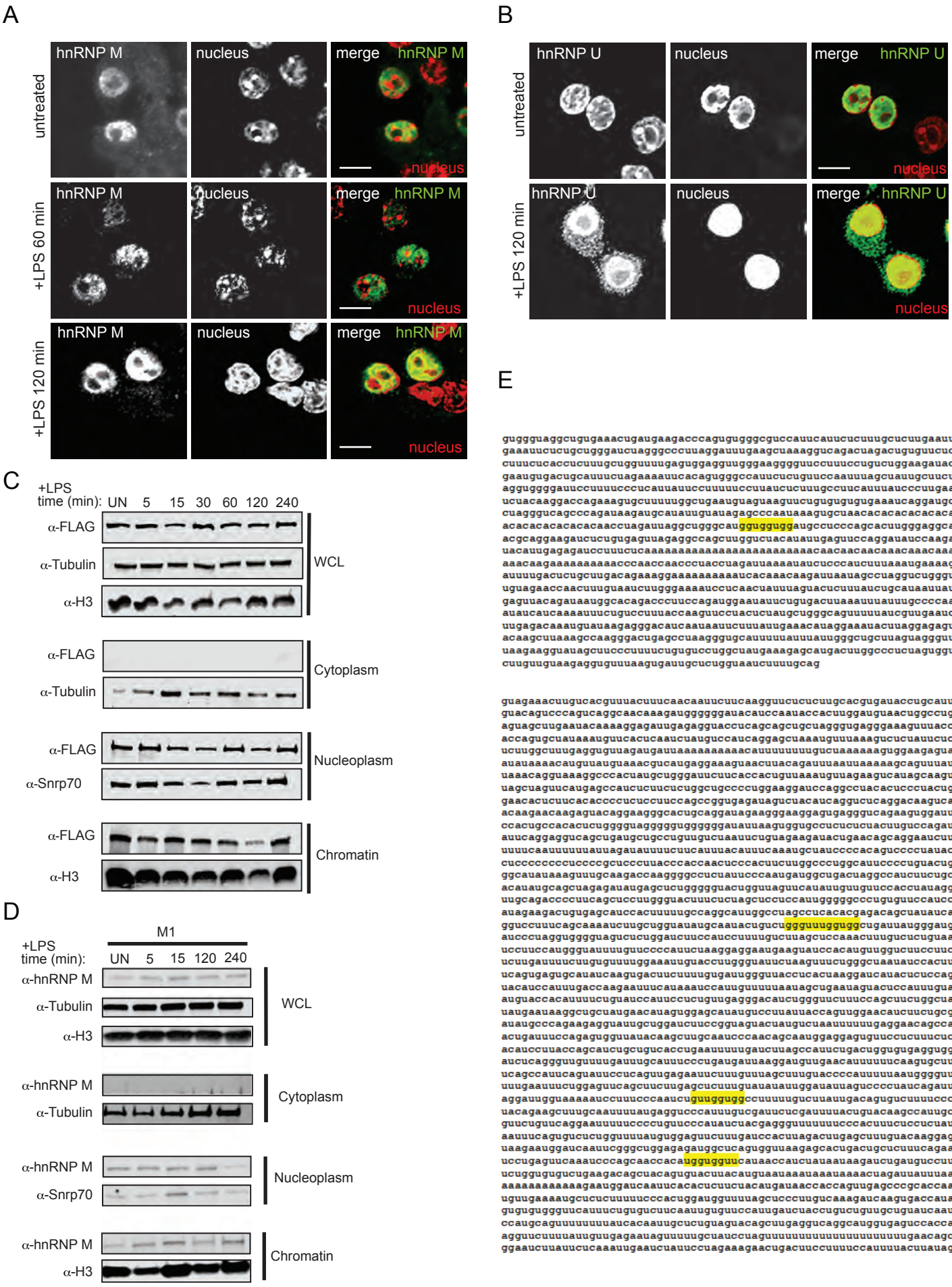

Supplemental Figure S4

Figure S4. Related to Figure 4. hnRNP M associates with chromatin at the *IL6* genomic locus. (a) Immunofluorescence microscopy of 3xFLAG-hnRNP M in untreated and LPS-treated macrophages (1hr and 2hr post-treatment). (b) Immunofluorescence microscopy of hnRNP U in untreated and LPS-treated macrophages (2hr post-treatment). (c) Western blot of whole cell lysate, cytoplasm, nucleoplasm, and chromatin of fractionated stable 3xFL-hnRNP M-expressing macrophages over a time-course of LPS treatment. (d) Western blot analysis of cellular fractions with anti-hnRNP M and loading controls of cytoplasm (tubulin), nucleoplasm (Snrp70) and chromatin (H3) fractions of uninfected and LPS stimulated hnRNP M KD 1 macrophages. (e) RNA sequence of *IL6* introns 2 and 3. Consensus or near-consensus hnRNP M binding sites are highlighted in yellow.

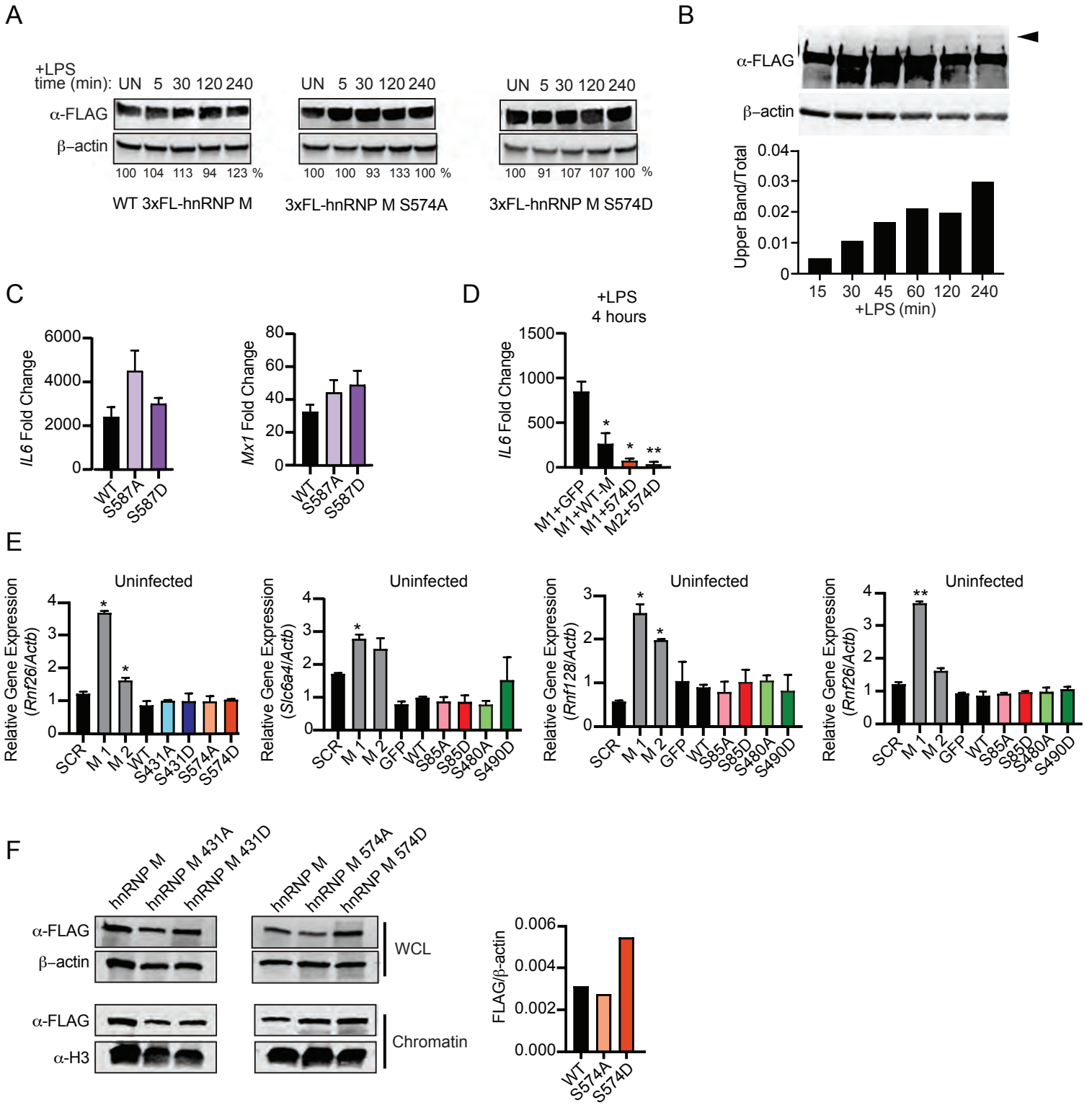

Figure S5. Related to Figure 5. Specific phosphorylation of hnRNP M controls its ability to repress expression of innate immune transcripts.

(a) Western blot analysis of 3xFL-hnRNP M WT, S574A, S574D phoshomutants stably expressed in RAW 264.7 macrophages treated with LPS for 5, 30, 120, and 240 mins. (b) Western blot analysis of phosphorylation events of 3xFL-hnRNP M WT stably expressed in RAW 264.7 macrophages treated with LPS for 15, 30, 45, 60, 120, and 240 mins. (c) IL6 and Mx1 expression by RT-qPCR, 2hr post-LPS treatment in 3xFL-hnRNP M WT and 3xFLhnRNP M S587A/D-expressing macrophages. (d) IL6 expression by RT-qPCR, 4hr post-LPS treatment in hnRNP M KD 1 macrophages complemented with 3xFL-GFP, 3xFL-hnRNP M WT, or S574D and hnRNP M KD 2 macrophages complemented with S574D. (e) Expression by RT-qPCR of Rnf26, Slc6a4, Rnf128 for 3xFL-hnRNP M WT, hnRNP M KD 1 and hnRNP M KD 2, and 3xFL-S431A/D, S574A/D, S85A/D, S480A/D-expressing macrophages. (f) Western blot of whole cell lysate and chromatin of fractionated stable 3xFL-hnRNP M WT, 3xFL-hnRNP M 431A/D and 3xFL-hnRNP M 574A/D-expressing macrophages. FLAG expression was quantified over βactin.

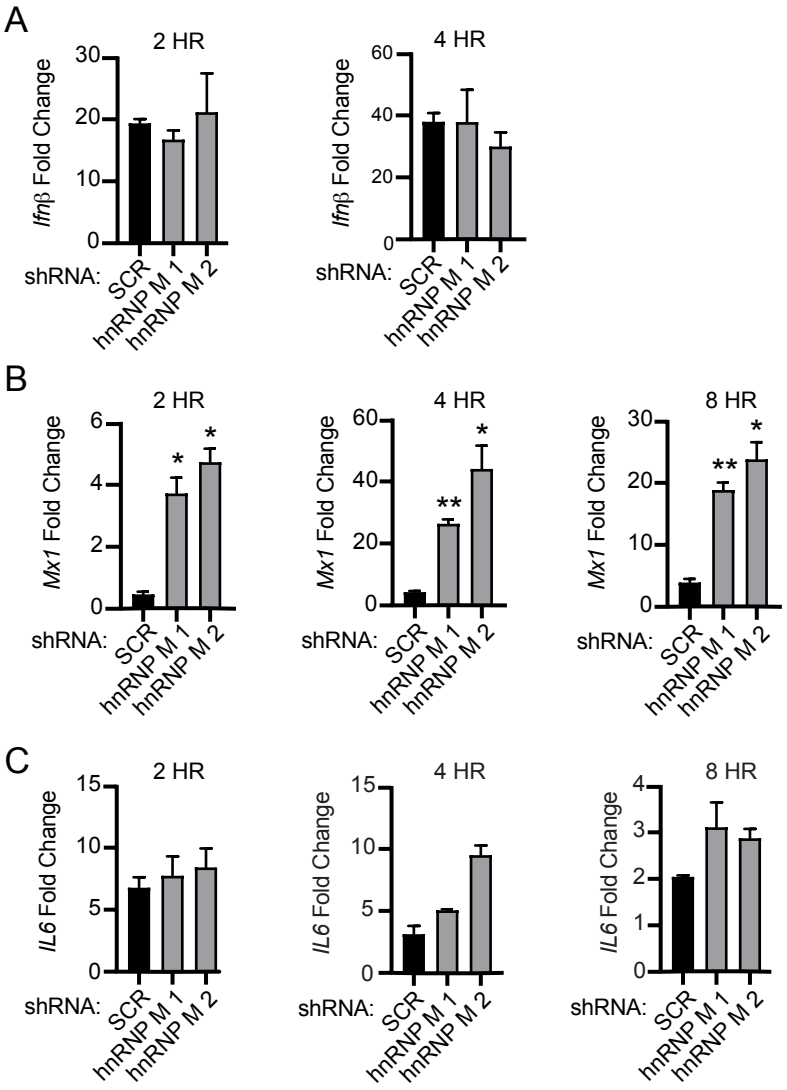

Figure S6. Related to Figure 6. hnRNP M influences innate immune gene expression during viral infection.
(a) RT-qPCR of Ifnβ mRNA levels in SCR control and hnRNP M KD cells at 2hr and 4hr post-infection, MOI=0.1. (b) RT-qPCR of Mx1 transcript in VSV infected SCR control and hnRNP M KD cells at 2hr, 4hr, and 8hr post-infection, MOI=0.1. (c) RT-qPCR of IL6 transcript in SCR control and hnRNP M KD cells at 2hr, 4hr, and 8hr post-infection, MOI=0.1. All figures are representative of 2 biological replicates.

A

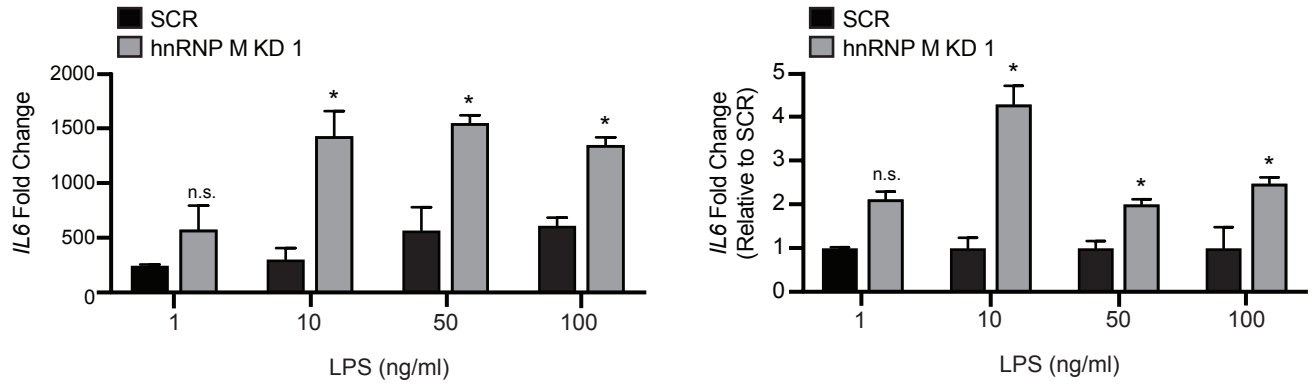

B

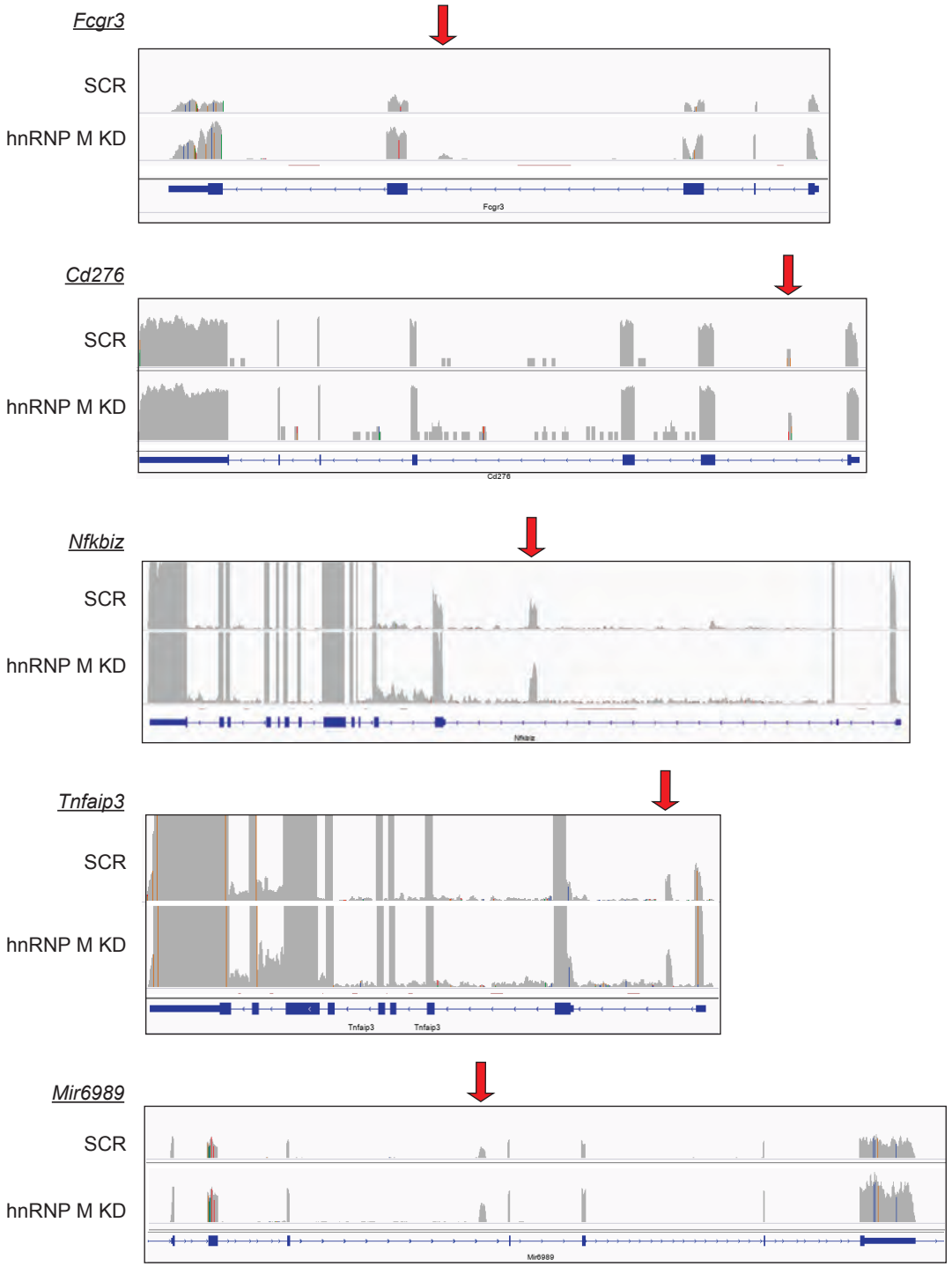

Supplemental Figure S7

Figure S7. Related to Figure 7. hnRNP M can respond to low levels of innate immune stimuli and may influence differential inclusion of cryptic exons.
(a) RT-qPCR of *IL6* mRNA levels in SCR control and hnRNP M KD cells at 2h treated with 100ng/ml, 50ng/ml, 10ng/ml and 1ng/ml. Data is expressed as fold-change over time = 0 as well as fold-change relative to SCR. (a) is representative of 2 biological replicates with values indicating means ± SD, n=2. Statistical significance was determined using two-tailed students' *t*-test. *P < 0.05, **P < 0.01, n.s.= not significant. (b) Screenshots of IGV viewer of *Salmonella*-infected SCR and hnRNP M KD RNA-Seq reads at *Fcgr3, Cd276, Nfkbiz, Tnfaip3,* and *Mir6989*. Red arrows indicate potential cryptic exons.

Primer: *Rnf26* F: AGAGCGGAAGAAGTGTGTTATC R: ATGAGGATCTCAGTGCAAGC
Primer: *Rnf128* F: CTTCAGTACAAGGAGCAGATGAG R: ATCCACGGCCACAGAATTT
Primer: *Slc6a* F: GTGTGTGAGGTTTAAGGTGAGTAG R: CAGAGGCCATTAGTGACATACC
Primer: *IL6* exon 1 F: GGGATGTCTGTAGCTCATTCTG R: AGAGGAACTTCATAGCGGTTTC
Primer: *IL6* intron 1 F: GCCCAACTGTGCTATCTGCT R: TCAGTCCCAAGAAGGCAACT
Primer: *IL6* exon 2 F: AGTTGCCTTCTTGGGACTGA R: GTCTCCTCTCCGGACTTGTG
Primer: *IL6* exon junction 1-2 F: GTCAATTCCAGAAACCGCTATG R: GGACTTGTGAAGTAGGGAAGG
Primer: *IL6* exon 2 F: TTGCCTTCTTGGGACTGATG R: TTAAGCCTCCGACTTGTGAAG
Primer: *IL6* intron 2 F: TGGTGCTTGTTGTAAGAGGTG R: TGCAAGTGCATCATCGTTGT
Primer: *IL6* exon junction 2-3 F: CTTCACAAGTCGGAGGCTTAAT R: GCAAGTGCATCATCGTTGTTC
Primer: *IL6* exon 3 F: GCAATGGCAATTCTGATTGTATGC R: ATCCAGTTTGGTAGCATCCATC
Primer: *IL6* intron 3 F: GAAAGAACTGACTTCCTTTTCCA R: GGTACTCCAGAAGACCAGAGGA
Primer: *IL6* exon 4 F: TTTCCTCTGGTCTTCTGGAGTA R: TGTATCTCTCTGAAGGACTCTGG
Primer: *IL6* intron 4 F: TGTGCAATATTTAACCAGTCTTTG R: GGAAATTGGGGTAGGAAGGA
Primer: *IL6* exon junction 3-4 F: GAAATGATGGATGCTACCAAACTG R: ACTCCAGAAGACCAGAGGAA
Primer: *IL6* exon 5 F: CCCAATTTCCAATGCTCTCCTA R: GGTTTGCCGAGTAGATCTCAAA
Primer: *IL6* exon junction 4-5 F: ACAAAGCCAGAGTCCTTCAG R: GTTAGGAGAGCATTGGAAATTGG

Primer: *Mx1* F: TCTGAGGAGAGCCAGACGAT R: ACTCTGGTCCCCAATGACAG
Primer: *TNF* F: ATGGCCTCCCTCTCATCAGT R: GTTTGCTACGACGTGGGCTA
Primer: *Gbp5* exon 4 F: AGGAGGCATCCAGGTCAAC R: TGTGTTCTCTATGGAAGGCAGA
Primer: *Ifnβ* set 1 F: GCAAGCTCAGGATCGCTATTA R: GGGACTCTTCCATCCTGAGT
Primer: *IRF7* F: CTTCAGCACTTTCTTCCGAGA R: TGTAGTGTGGTGACCCTTGC
Primer: *Commd8* F (exon 3): TGAGTGGAAGCATGTTCTCG R (exon 5): GCTGCGCACAAGAAATATCA
Primer: *Nmt2* F (exon 3): CATCTGGCAGCAGATTTCAG R (exon 5): GTGGCCTCATCAATGTTCCT
Primer: *IFIT* F: AGCTTTAGGGCAAGGAGAAC R: CGTAGCCTATCGCCAAGATTTA
Primer: *hnRNP M* KD check F: TTTGACCGAGCCATTGAGAT R: CTTCCTGGCTACTCCAGGTG
Primer: *Adora2a* set 3 F: GCTATTGCCATCGACAGATACA R: GTACCACGTCCTCAAACAGAC
Primer: *Marcks* set 2 F: GTGCCCAGTTCTCCAAGAC R: TTTACGTGGCCATTCTCCTG
CHIP Primer: IL6 1 F: CAGCAGTGGGATCAGCACTAA R: CCCAGTGGTCTCTTGGCTATC
CHIP Primer: IL6 2 F: TGAGGCTAGCCCTAAGAAGCA R: CCATCAAGACATGCTCAAGTGC
CHIP Primer: IL6 3 F: GAAAACCGGCAAGTGAGCAG R: CCTCTGGCGGAGCTATTGAG
CHIP Primer: IL6 4 F: TTTGAGTGGAGGTTGGGAAGG R: TGAGGGAAAAGGAATCCCCAC
CHIP Primer: IL6 5 F: TTTGACTCTGCTTGACAGAAAGG R: TGGTTCTACACACCCAGACCT
CHIP Primer: IL6 6 F: AACGATGATGCACTTGCAGA R: ACGTGCAAGAGAGAACCTTGA

CHIP Primer: IL6 7 F: ACAGGTAAAGGCCCACTATGC R: GTGTAGGCCTGGATCCTTCC
CHIP Primer: IL6 8 F: GGGAAGGAGTGAGGGTCAGAA R: GCATCAGCTGACCTCCTGAATTA
CHIP Primer: IL6 9 F: TCCCTAGGTGGGGTAGTCTC R: GGGGAACAAAATACCCATGGAAG
CHIP Primer: IL6 end F: AGTGGCAGACAGAACAGTAAGG R: TTTGACTCACCCAAGCCAGG
CHIP Primer: Intergenic Control F: ATTTTGTGCTGCATAACCTCCT R: TAGCAACATCCTAAGCTGGACA
Primer: VSV-G F: CAAGTCAAAATGCCCAAGAGTCACA R: TTTCCTTGCATTGTTCTACAGATGG
Primer: VSV-M F: ATGATCCGAATCAATTAAGATATG R: GGGACGTTTCCCTGCCATTCCGATG
Primer: shRNA pSICO SCR: F: TCCTAGGTTAAGTCGCCCTTTCAAGAGATAGA AGGGCGACTTAACCTAGGTTTTTTC R: TCGAGAAAAAACCTAGGTTAAGTCGCCCTTCTCTTGAA AGGGCGACTTAACCTAGGA
Primer: shRNA hnRNP M1: F: TGGAAGATGCTAAAAGGACAATTCAAGAGATTGTCCTT TAGCATCTTCCTTTTTTC R: TCGAGAAAAAAGGAAGATGCTAAAGGACAATCTCTTGA ATTGTCCTTTAGCATCTTCC
Primer: shRNA hnRNP M2: F: TGCACAGTATTTGTAGCAAATTCAAGAGATTTGCTAC AAATACTGTGCTTTTTTC R: TCGAGAAAAAAGCACAGTATTTGTAGCAAATCTCTTGAA TTTGCTACAAATACTGTGC

Table S4